

Bounds on Lorentz-violating Yukawa couplings via lepton electromagnetic moments

J. Alfonso Ahuatzí-Avendaño,¹ Javier Montaña,² Héctor Novales-Sánchez¹,¹ Mónica Salinas,¹ and J. Jesús Toscano¹

¹*Facultad de Ciencias Físico Matemáticas, Benemérita Universidad Autónoma de Puebla, Apartado Postal 1152 Puebla, Puebla, México*

²*Cátedras Conacyt-Facultad de Ciencias Físico Matemáticas, Universidad Michoacana de San Nicolás de Hidalgo, Avenida Francisco J. Múgica s/n, C.P. 58060, Morelia, Michoacán, México*



(Received 27 August 2020; revised 4 February 2021; accepted 8 February 2021; published 2 March 2021)

The effective-Lagrangian description of Lorentz-invariance violation provided by the so-called Standard Model extension covers all the sectors of the Standard Model, allowing for model-independent studies of high-energy phenomena that might leave traces at relatively low energies. In this context, the quantification of the large set of parameters characterizing Lorentz-violating effects is well motivated. In the present work, effects from the Lorentz-nonconserving Yukawa sector on the electromagnetic moments of charged leptons are calculated, estimated, and discussed. Following a perturbative approach, explicit expressions of leading contributions are derived, and upper bounds on Lorentz violation are estimated from current data on electromagnetic moments. Scenarios regarding the coefficients of Lorentz violation are considered. In a scenario of two-point insertions preserving lepton flavor, the bound on the electron electric dipole moment yields limits as stringent as 10^{-27} , whereas muon and tau-lepton electromagnetic moments determine bounds as restrictive as 10^{-14} and 10^{-5} , respectively. Another scenario defined by the assumption that Lorentz-violating Yukawa couplings are Hermitian leads to less stringent bounds provided by the muon anomalous magnetic moment, which turn out to be as restrictive as 10^{-14} .

DOI: [10.1103/PhysRevD.103.055003](https://doi.org/10.1103/PhysRevD.103.055003)

I. INTRODUCTION

It has been half a century since its formulation [1–3], and yet the Standard Model (SM) remains our best theoretical description of fundamental physics [4]. Even so, the SM is nowadays considered by the scientific community to be a low-energy manifestation of an underlying theory operating at some very-high-energy scale, perhaps of the order of the Planck scale. In general, the two main ingredients behind the definition of field theories are their dynamic variables and symmetries [5]. Regarding the latter aspect, invariance under spacetime and gauge transformations have traditionally received much attention in model building. While Lorentz symmetry is a conventional assumption in beyond-SM contexts, Planck-scale physical formulations, such as string theory and noncommutative field theory, are able to spontaneously brake it [6–9], thus yielding Lorentz-nonconserving physical phenomena which, at current experimental sensitivity, may manifest as measurable tiny

effects. Since no compelling evidence of Lorentz violation has been ever observed [10], thus leaving us blind as to which place is the best to introduce this kind of new physics, the effective-Lagrangian approach [5,11], distinguished for being model independent, seems to be suitable.

A couple of decades ago, an effective-Lagrangian description of Lorentz-symmetry nonconservation known as the Lorentz- and *CPT*-violating SM extension (SME) was devised [12,13]. The SME has since become a useful tool to comprehensively study this sort of new physics,¹ which induces unconventional phenomena such as vacuum birefringence [15,16], vacuum Čerenkov radiation [17–22], oscillations of massless neutrinos [23–26], exotic electromagnetic properties of SM particles [27,28], and violations of standard theorems [29,30]. The dynamic variables of the SME and its gauge-symmetry group are the same as those of the sole SM, the key element being a large set of coefficients characterized by fully contracted spacetime indices within Lagrangian terms and which transform as tensors under observer Lorentz transformations [12,13], thus implying that Lorentz-violating physics is observer independent. Nonetheless, these tensor coefficients, which define preferred directions in spacetime, are invariant under

Published by the American Physical Society under the terms of the Creative Commons Attribution 4.0 International license. Further distribution of this work must maintain attribution to the author(s) and the published article's title, journal citation, and DOI. Funded by SCOAP³.

¹The SME is nicely and succinctly reviewed in Ref. [14].

particle Lorentz transformations [12,13], so they do not preserve Lorentz symmetry. The estimation of the quite vast set of SME coefficients has become the main objective of several phenomenological investigations of Lorentz violation. The present paper is one of such works. A comprehensive catalog of SME-coefficients constraints is provided in Ref. [10], which, moreover, is updated every year. Lorentz-violating Lagrangian terms constituting the SME are classified into two types, according to whether they are power-counting renormalizable or not [16,27,28,30–35]. The full set of renormalizable SME terms define the so-called minimal SME (MSME). Within the framework of the MSME, the present paper is a phenomenological investigation of effects of Lorentz violation of the anomalous magnetic moments (AMMs) a_A and electric dipole moments (EDMs) d_A of charged leptons l_A , with $A = e, \mu, \tau$ labeling lepton flavors. The emergence of contributions to these electromagnetic moments as by-products of Lorentz-invariance nonconservation has been addressed by the authors of Refs. [27,28,36–41]. Under the assumption of Lorentz invariance, contributions to AMMs and EDMs are identified from the well-known parametrization of the electromagnetic vertex $A_\mu l_A l_A$ given by $\bar{u}_A(p')\Gamma_\mu u_A(p)$, with u_A the momentum-space Dirac spinor for a charged lepton l_A with mass m_A , and Γ_μ given by [42–44]

$$\Gamma_\mu = ie \left[\gamma^\mu (f_A^V - f_A^A \gamma_5) - \sigma_{\mu\nu} q^\nu \left(i \frac{f_A^m}{2m_A} - \frac{f_A^d}{e} \gamma_5 \right) \right], \quad (1)$$

for on-shell external fermions and off-shell photon field, in which case all form factors, particularly the magnetic form factor $f_A^a(q^2)$ and the electric form factor $f_A^d(q^2)$, are functions of squared transferred momentum q^2 only. The on-shell-photon case, in which $q^2 = 0$, defines the AMM and the EDM by $a_A \equiv f_A^a(q^2 = 0)$ and $d_A \equiv f_A^d(q^2 = 0)$, respectively. While in the presence of Lorentz violation the structure of the corresponding electromagnetic interaction parametrization is expected to be far richer [27,28], AMMs and EDMs are still identified from the aforementioned Lorentz-preserving parametrization. Therefore, AMMs and EDMs from Lorentz violation necessarily originate in second-order SME-coefficients contributions, since in such a case form-factor contributions with fully contracted spacetime indices may emerge.

Lorentz-violating effects addressed in the present work emerge from the Yukawa sector of leptons in the MSME, where both flavor and spacetime indices characterize Yukawa-like Lorentz-violating constants. Lorentz violation from these interactions is introduced in the Feynman-diagrams approach through three-point vertices and from two-point insertions as well, with both elements including lepton-flavor change. We emphasize, though, that transition electromagnetic moments [43,44] are not within the scope of the present work, so external fermion lines are always taken to preserve lepton flavor. Leading contributions to the

electromagnetic form factors of interest are generated by Feynman diagrams with a virtual-photon line, which dominate over contributions from diagrams in which either Higgs or Z bosons participate. In this context, current AMMs and EDMs data are utilized to estimate upper bounds on SME coefficients. Since the resulting contributions involve a plethora of Lorentz-violation parameters, assumptions aiming at the reduction of the number of SME quantities are made, for which two scenarios are considered. In one of these scenarios, some SME parameters introduced by lepton-flavor-nonconserving two-point insertions are assumed to be quite small, thus being disregarded and then leaving appropriate conditions to bound Lorentz-violation coefficients to be as small as 10^{-27} , from the electric dipole moment of the electron, and limits as restrictive as 10^{-14} and 10^{-5} if constraints on the muon and the tau-lepton electromagnetic moments, respectively, are taken into account. Another scenario, relying on the assumption that Yukawa-like-related couplings are Hermitian, also gives rise to bounds on SME coefficients. In this scenario, the analysis of MSME contributions and their comparison with current bounds on electromagnetic moments of charged leptons determine upper limits on the impact of Lorentz-violating coefficients as stringent as 10^{-15} , which, specifically, are imposed by the anomalous magnetic moment of the muon. In the same scenario, SME contributions to electric dipole moments are absent. A table summarizing these bounds is provided in this section.

The remainder of the paper has been organized as follows. In Sec. II, a brief discussion on the theoretical framework necessary for the phenomenological calculation is performed. We present in Sec. III the analytical calculation of the electromagnetic vertex $A_\mu l_A l_A$ at one loop. Numerical estimations and a discussion on our results are provided in Sec. IV. Finally, we give a summary of the present investigation in Sec. V.

II. LORENTZ VIOLATION IN THE YUKAWA SECTOR

Since the MSME is an effective field theory parametrizing heavy physics at SM energy scales, its Lagrangian terms are exclusively defined in terms of the fields of such a low-energy description. In this context, Lorentz-nonconserving interactions are introduced in all the SM sectors, among which we consider, for the phenomenological objectives of the present investigation, Lagrangian terms from the Yukawa sector. Meanwhile, $SU(3)_C \times SU(2)_L \times U(1)_Y$ gauge symmetry is still assumed and then spontaneously broken through implementation of the Brout-Englert-Higgs mechanism [45–47] as usual, in order to define the full set of mass eigenfields within the theory governed by the electromagnetic gauge group [48–52]. Of course, this procedure affects Lorentz-violating interactions, for which a discussion on the resultant terms of the MSME Yukawa sector is pertinent.

In the MSME, the Yukawa sector is CPT even and is given by [13]

$$\begin{aligned} \mathcal{L}_Y = & -(Y_L)^{AB} \bar{L}_A \phi R_B - \frac{1}{2} (H_L)_{\mu\nu}^{AB} \bar{L}_A \phi \sigma^{\mu\nu} R_B \\ & - (Y_U)^{AB} \bar{Q}_A \tilde{\phi} U_B - \frac{1}{2} (H_U)_{\mu\nu}^{AB} \bar{Q}_A \tilde{\phi} \sigma^{\mu\nu} U_B \\ & - (Y_D)^{AB} \bar{Q}_A \phi D_B - \frac{1}{2} (H_D)_{\mu\nu}^{AB} \bar{Q}_A \phi \sigma^{\mu\nu} D_B + \text{H.c.} \quad (2) \end{aligned}$$

Here, ϕ is the Higgs doublet. Moreover, L_A and R_A are the SM $SU(2)_L$ left-handed lepton doublets and right-handed lepton singlets, respectively. Q_A , on the other hand, are the right-handed quark doublets, whereas U_A are the u -type quark singlets, and D_A are the d -type quark singlets, both right-handed. In all cases, capital letter indices A, B label fermion flavor. The matrices with entries $(H_L)_{\mu\nu}^{AB}$, $(H_U)_{\mu\nu}^{AB}$, $(H_D)_{\mu\nu}^{AB}$ are dimensionless, but, as it happens with the SM Yukawa matrices Y_L, Y_U, Y_D , they are not restricted to be Hermitian in flavor space. This opens a window to look for flavor-violation effects mediated by the Higgs boson. A thorough discussion on this Lorentz-violating Yukawa sector, which includes its application to the photon propagator within the scheme of nonlinear covariant gauges [53–56], was recently carried out in Ref. [57]. Notation and conventions utilized in the present paper have been taken from that reference.

After spontaneous symmetry breaking, and once implementation of the standard unitary transformations to pass from the gauge basis to the basis of mass eigenstates has been performed, the Lagrangian given in Eq. (2) can be written in the unitary gauge as

$$\begin{aligned} \mathcal{L}_Y = & -\sum_A \left(m_{f_A} + \frac{g m_{f_A}}{2 m_W} H \right) \bar{f}_A f_A \\ & - \frac{1}{2} \sum_{A,B} (v + H) \bar{f}_A (V_{\alpha\beta}^{AB} + A_{\alpha\beta}^{BA*} \gamma^5) \sigma^{\alpha\beta} f_B, \quad (3) \end{aligned}$$

where

$$V_{\alpha\beta}^{AB} = \frac{1}{2} (Y_{\alpha\beta}^{AB} + Y_{\alpha\beta}^{BA*}), \quad (4)$$

$$A_{\alpha\beta}^{AB} = \frac{1}{2} (Y_{\alpha\beta}^{AB} - Y_{\alpha\beta}^{BA*}). \quad (5)$$

In the above expressions, $Y_{\alpha\beta} = V_L^\dagger H_{\alpha\beta} V_R$, with V_L and V_R the unitary matrices connecting the gauge and mass-eigenfields bases of chiral spinors. Though not explicitly indicated by the notation of matrices $Y_{\alpha\beta}$, three types of fermions correspond to each of them, namely, $Y_{\alpha\beta}^L, Y_{\alpha\beta}^U$, and $Y_{\alpha\beta}^D$, which stand for charged leptons, u -type quarks, and d -type quarks, respectively. With respect to flavor space, matrices $V_{\alpha\beta}$ are Hermitian, whereas matrices $A_{\alpha\beta}$ are

anti-Hermitian. On the other hand, matrices V^{AB} and A^{AB} given in spacetime group are both antisymmetric. In the perturbative approach, which is adopted here, these Lorentz-violating Yukawa couplings yield two types of physical couplings: the bilinear insertion $-(v/2) \bar{f}_A (V_{\alpha\beta}^{AB} + A_{\alpha\beta}^{BA*} \gamma^5) \sigma^{\alpha\beta} f_B$ and the trilinear vertex $-(1/2) H \bar{f}_A (V_{\alpha\beta}^{AB} + A_{\alpha\beta}^{BA*} \gamma^5) \sigma^{\alpha\beta} f_B$. For instance, the one-loop contribution from this sort of Lorentz violation to the photon propagator is determined by the bilinear term, whose Feynman rule is $-i(v/2)(V_{\alpha\beta}^{AB} + A_{\alpha\beta}^{BA*} \gamma^5) \sigma^{\alpha\beta}$ [57]. Note that from Eq. (5), $A_{\alpha\beta}$ vanishes for Hermitian matrix $Y_{\alpha\beta}^\dagger = Y_{\alpha\beta}$, whereas the anti-Hermitian-matrix condition $Y_{\alpha\beta}^\dagger = -Y_{\alpha\beta}$ eliminates $V_{\alpha\beta}$.

III. ONE-LOOP CONTRIBUTIONS TO LEPTON ELECTROMAGNETIC INTERACTIONS

Next we calculate the contributions from Lorentz violation in the Yukawa sector \mathcal{L}_Y , Eq. (3), to the electromagnetic vertex $A_\mu f_A f_A$. To execute this task, we follow a perturbative approach, in which the effects from Lorentz-violating Lagrangian terms that are quadratic in fields are taken into account by placing two-point vertex insertions in propagator lines of Feynman diagrams. This *modus operandi* has been of profit in previous phenomenological investigations [27–30,36,37,57–61].

As explicitly shown in Refs. [27,28], electromagnetic interactions at the loop level are modified by the occurrence of Lorentz violation, resulting in a larger number of electromagnetic form factors than those in Eq. (1), constructed under the assumption of Lorentz invariance [42–44]. Nevertheless, even if Lorentz symmetry is violated, the form factors defining the AMM and the EDM are to be identified from the Lorentz-invariant contributions of Eq. (1), where Lorentz-violating background fields can only be contracted with themselves. According to Eq. (3), the coefficients $V_{\mu\nu}^{AB}$ and $A_{\mu\nu}^{AB}$ are antisymmetric with respect to spacetime indices, so they are traceless in this sense. Consequently, any first-order contribution to AMMs and EDMs vanishes. But note that nonzero Lorentz-invariant contributions may emerge as long as diagrams at the second order in $V_{\mu\nu}^{AB}$ or $A_{\mu\nu}^{AB}$ are considered.

A. Contributing Feynman diagrams

With the previous discussion in mind, we consider the contributions to the electromagnetic vertex $A_\mu f_A f_A$ produced by the sum of the Feynman diagrams shown in Figs. 1 and 2, in which either two two-point insertions or two three-point vertices or simultaneously one two-point insertion and one three-point vertex appear, thus resulting in second-order contributions of MSME coefficients. The full set of contributing diagrams can be classified into three types: diagrams with a virtual Z -boson line, diagrams with a virtual-photon line, and diagrams with a virtual

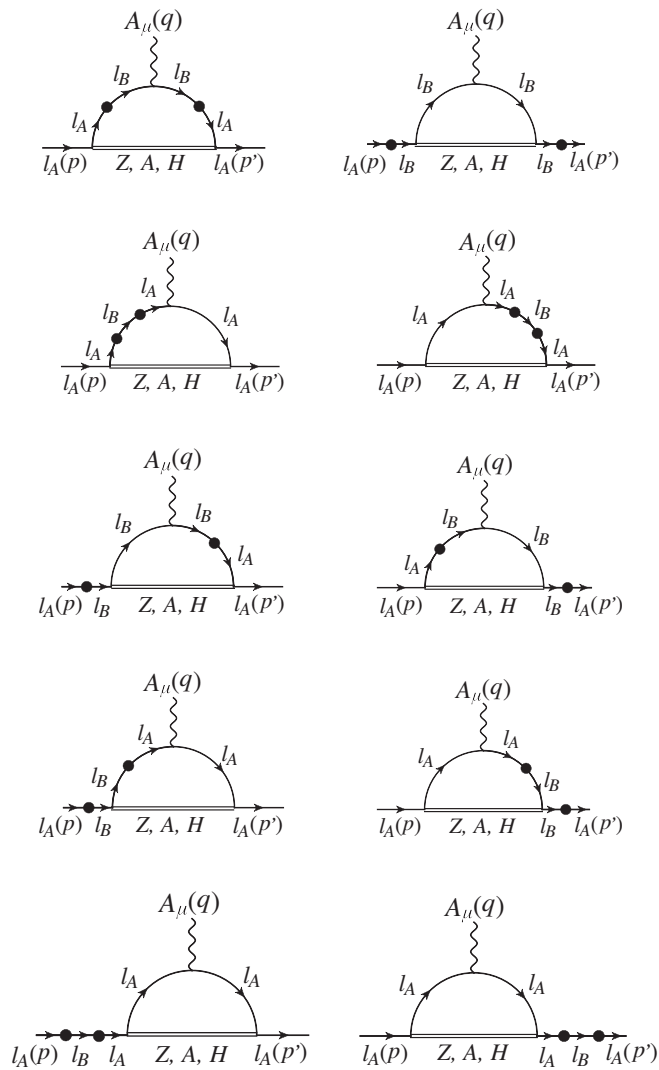


FIG. 1. Feynman diagrams $A_{\mu} f_A f_A$ contributing to magnetic and electric form factors, with Lorentz-nonconservation effects entering exclusively through bilinear insertions $l_A l_B$, where either $A = B$ or $A \neq B$. Virtual double lines in loops stand for a Z boson, a photon, or a Higgs boson.

Higgs-boson line. Neutrinos are assumed to be massless, so no couplings among them and the Higgs field arise, with the consequence that no contributing diagrams with virtual W -boson lines exist. Double lines in the loops of diagrams of Fig. 1 generically represent virtual-field lines which can be associated with either a Z boson, a photon, or a Higgs boson. This figure displays the whole set of Feynman diagrams in which a virtual Z boson or a virtual photon participate. Vertices $H f_A f_B$ involving the coefficients $V_{\mu\nu}^{AB}$ and $A_{\mu\nu}^{AB}$ emerge from Eq. (3), thus giving rise to the diagrams of Fig. 2, which add together with diagrams comprising bilinear insertions, comprehended by Fig. 1, to give the full set of diagrams with Higgs-boson loop lines. We find it worth emphasizing that both two-point insertions and three-point vertices generated by Eq. (3) are

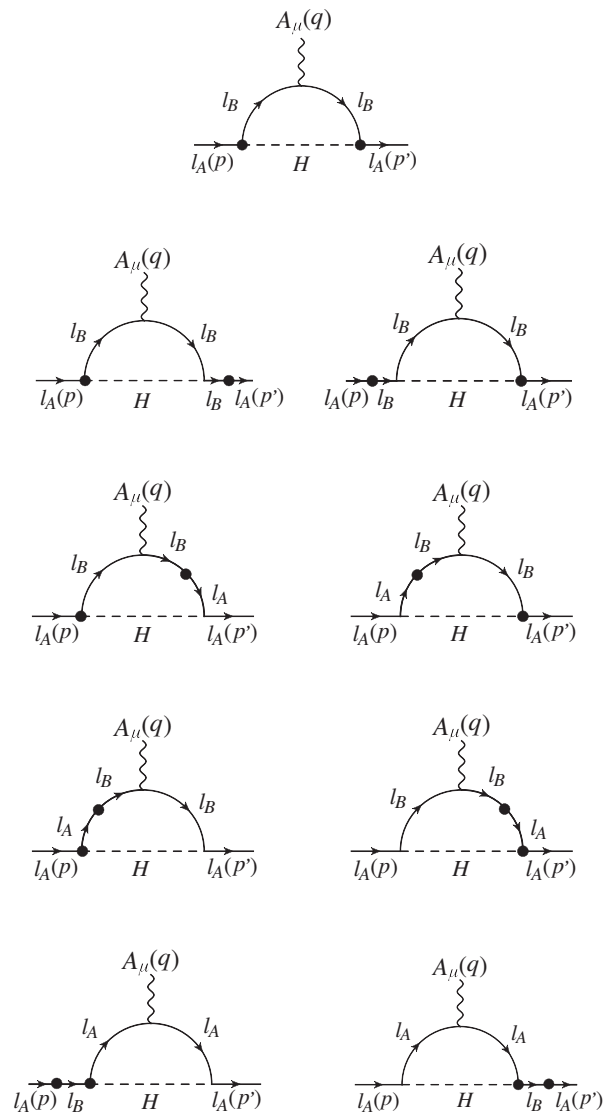


FIG. 2. Feynman diagrams $A_{\mu} f_A f_A$ contributing to magnetic and electric form factors, with Lorentz-nonconservation effects entering through both bilinear insertions $l_A l_B$ and three-point vertices $H f_A f_B$, where either $A = B$ or $A \neq B$. These diagrams require the presence of a virtual Higgs-boson line in order to exist.

flavor changing, which enlarges the number of contributing diagrams. Also notice that the calculation is performed in the unitary gauge, so no diagrams with pseudo-Goldstone bosons exist.

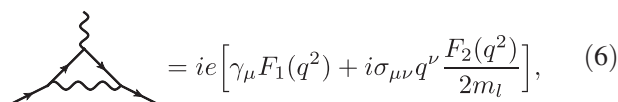
We have performed all the calculations by following the Passarino-Veltman tensor-reduction method [62], for which the software *Mathematica*, by Wolfram, has been utilized, together with the packages *FeynCalc* [63] and *Package-X* [64]. After carrying out these calculations and organizing the resulting expressions, we identified the contributions from each set of diagrams in Figs. 1 and 2 to AMMs and EDMs. The occurrence of two-point insertions in contributing Feynman diagrams comes along with technical

complications. The presence of Lorentz-violating coefficients, which cannot be simplified by on-shell conditions, diversifies the set of different Lorentz structures participating in the loop contributions. For the same reason, the expressions for the generated form factors are quite large, even though this is an on-shell calculation performed in a specific gauge. Under such circumstances, for us it made no sense to provide the explicit expressions of the AMMs and EDMs contributions. Nonetheless, using Package-X, we were able to numerically check the consistent cancellation of ultraviolet (UV) divergences in all the contributions. Another practical complication arises because each bilinear insertion introduces an extra loop denominator, so loop integrals involve several propagator denominators, for which calculation strategies were realized and implemented.

B. Dominant contributions to electromagnetic moments

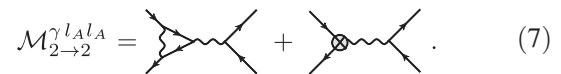
The calculation of the electromagnetic vertex $A_\mu l_A l_A$ is carried out by taking both external fermions on shell, but keeping the photon field off shell, so that $q^2 \neq 0$ (see Figs. 1 and 2 for notation). We classify contributing diagrams into two sets: (1) diagrams where bilinear insertions or three-point vertices involve change of lepton flavor, that is with $A \neq B$, which we refer to as the case of virtual-lepton-flavor change, and (2) diagrams in which no lepton-flavor change occurs due to two-point insertions or three-point vertices, that is $A = B$, which we call the case of virtual-lepton-flavor conservation. The leading contributions to AMMs and EDMs are produced by diagrams with a virtual-photon line provided in Fig. 1. Quantitatively, the difference between such dominant contributions and those arising from other diagrams is 10 orders of magnitude at least. While all diagrams, of all sorts, have been calculated and their contributions estimated, we explain the techniques involved in the calculations by specifically discussing the aforementioned leading contributions in some detail.

Virtual-photon diagrams come along with infrared (IR) divergences, which motivates us to introduce a fictitious photon mass, m_γ [48,52]. An aspect worth commenting on is that diagrams with two two-point insertions on a single virtual-fermion line generate IR divergences, whereas diagrams in which propagators involve exactly one such insertion are IR finite. For a moment, consider in the context of the Lorentz-invariant SM, the electromagnetic vertex $A_\mu l_A l_A$ at one loop. The contributions from quantum electrodynamics to this vertex are parametrized as



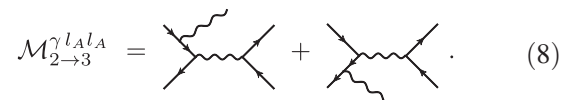
$$\text{Diagram} = ie \left[\gamma_\mu F_1(q^2) + i \sigma_{\mu\nu} q^\nu \frac{F_2(q^2)}{2m_l} \right], \quad (6)$$

where the form factor $F_1(q^2)$ involves UV divergences as well as IR divergences, whereas the magnetic form factor $F_2(q^2)$ is finite in both senses. IR divergences are not eliminated directly from the amplitude of this contribution, but they are rather eradicated at the cross-section level. For instance, consider the quantum-electrodynamics contributions to the process $l_A^+ l_A^- \rightarrow l_B^+ l_B^-$. The corresponding amplitude can be written as $\mathcal{M}_{2 \rightarrow 2} = \mathcal{M}_{2 \rightarrow 2}^{\text{tree}} + \mathcal{M}_{2 \rightarrow 2}^{\text{loop}}$, where $\mathcal{M}_{2 \rightarrow 2}^{\text{tree}}$ and $\mathcal{M}_{2 \rightarrow 2}^{\text{loop}}$ are the tree-level contribution and the loop contributions, respectively. We conveniently express the loop-amplitude contribution as $\mathcal{M}_{2 \rightarrow 2}^{\text{loop}} = \mathcal{M}_{2 \rightarrow 2}^{\gamma l_A l_A} + \dots$, with



$$\mathcal{M}_{2 \rightarrow 2}^{\gamma l_A l_A} = \text{Diagram 1} + \text{Diagram 2}. \quad (7)$$

The second diagram in Eq. (7), standing for the counterterm for the first one, is introduced as part of the procedure of renormalization. The differential-cross-section contribution $d\sigma_{2 \rightarrow 2}^{\text{interf.}} \propto \sum_{\text{spin}} [(\mathcal{M}_{2 \rightarrow 2}^{\text{tree}})^* \mathcal{M}_{2 \rightarrow 2}^{\gamma l_A l_A} + \mathcal{M}_{2 \rightarrow 2}^{\text{tree}} (\mathcal{M}_{2 \rightarrow 2}^{\gamma l_A l_A})^*]$ of interference terms still bears IR divergences, so this quantity is not observable. On the other hand, think of the bremsstrahlung process $l_A^+ l_A^- \rightarrow \gamma l_B^+ l_B^-$ under the assumption that the final-state photon is soft. The tree-level amplitude is expressed as $\mathcal{M}_{2 \rightarrow 3}^{\text{tree}} = \mathcal{M}_{2 \rightarrow 3}^{\gamma l_A l_A} + \dots$, where



$$\mathcal{M}_{2 \rightarrow 3}^{\gamma l_A l_A} = \text{Diagram 1} + \text{Diagram 2}. \quad (8)$$

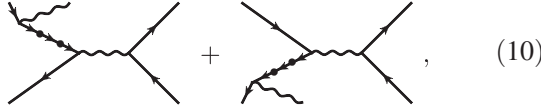
The corresponding differential cross section $d\sigma_{2 \rightarrow 3} = d\sigma_{2 \rightarrow 3}^{\gamma l_A l_A} + \dots$ with $d\sigma_{2 \rightarrow 3}^{\gamma l_A l_A} \propto \sum_{\text{spin}} |\mathcal{M}_{2 \rightarrow 3}^{\gamma l_A l_A}|^2$ turns out to be IR divergent. At the end of the day, the sum $d\sigma_{2 \rightarrow 2}^{\text{interf.}} + d\sigma_{2 \rightarrow 3}^{\gamma l_A l_A}$ with the assumption of soft photon emission in $l_A l_A \rightarrow \gamma l_B l_B$ yields an IR finite contribution. In other words, IR divergences that originated in the amplitudes given by Eqs. (7) and (8) cancel each other when taking the two cross sections together. It is important to emphasize that the bremsstrahlung diagrams of Eq. (8) are constructed by insertion of the electromagnetic vertex, only proportional to γ_μ , in a external line of some tree-level diagram $l_A l_A \rightarrow l_B l_B$. Such a Dirac matrix is just the one appearing in the IR-divergent form factor $F_1(q^2)$ in Eq. (6). In the case of the MSME contributions considered for the present investigation, IR divergences arise in the magnetic and in the electric form factors proportional to 4×4 matrices $\sigma_{\mu\nu}$ and $\sigma_{\mu\nu} \gamma_5$, respectively, defined in the space of Dirac matrices. This means that such form factors are not measurable quantities. We argue that, analogous to the Lorentz-conserving case, such IR divergences should vanish at the level of cross section, with the complicity of bremsstrahlung diagrams involving Lorentz-violating bilinear insertions.

To illustrate this, consider the one-loop Lorentz-violating amplitude of $l_A l_A \rightarrow l_B l_B$, which, among the whole set of contributing Feynman diagrams, receives contributions from the IR-divergent sum



$$(9)$$

At tree level, the bremsstrahlung diagrams



$$(10)$$

bearing effects of violation of Lorentz invariance induced by SME bilinear insertions, contribute to $l_A l_A \rightarrow \gamma l_B l_B$. A soft final-state photon is assumed here as well. Both sums of diagrams being IR divergent and proportional to matrices $\sigma_{\mu\nu}$ and $\sigma_{\mu\nu}\gamma_5$ are expected to produce contributions to differential cross sections which, summed together, should cancel all IR divergences, thus resulting in a finite total cross section. The proof of this statement is beyond the scope of the present paper, while it is left for a future ongoing investigation.

For a variety of models, analytic expressions of triangle diagrams written in the unitary gauge bear three propagator denominators. Nonetheless, the use of two-point insertions in the present calculation yields expressions with up to five such denominators. We have executed this calculation by following two different paths, and we have verified that the results obtained through both approaches coincide with each other. One such approach consists of a direct calculation in which four- and five-point Passarino-Veltman scalar functions [62] emerge. In the other method, which we discuss in detail next, the number of propagator denominators in loop integrals is reduced to just three by implementing a trick involving squared-mass derivatives. Consider the first, third, and fourth diagrams of Fig. 1 in the case of the virtual-photon line. These diagrams, which have been identified to produce the leading contributions among the whole set of virtual-photon diagrams, have Lorentz-violating two-point insertions in loop lines exclusively. After defining $\Delta_\gamma = k^2 - m_\gamma^2$ and $\Delta_j(p) = (k+p)^2 - m_j^2$, and implementing the Feynman parameters technique [48,65], we write the analytical expressions of these diagrams as

$$\Gamma_{1\mu}^{AB} = \frac{i}{(4\pi)^2} \frac{(2\pi\mu)^{4-D}}{i\pi} \int d^D k \times \int_0^1 dx dy \frac{\partial^2}{\partial m_j^2 \partial m_k^2} \frac{N_{1\mu}(m_A, m_B)}{\Delta_\gamma \Delta_j(l) \Delta_k(l')} \Bigg|_{\substack{m_j=m_A \\ m_k=m_B}}, \quad (11)$$

$$\Gamma_{2\mu}^{AB} = \frac{i}{(4\pi)^2} \frac{(2\pi\mu)^{4-D}}{i\pi} \int d^D k \times \int_0^1 dx \frac{\partial^2}{\partial (m_j^2)^2} \frac{x N_{2\mu}(m_A, m_B)}{\Delta_\gamma \Delta_j(l) \Delta_B(p)} \Bigg|_{m_j=m_A}, \quad (12)$$

$$\Gamma_{3\mu}^{AB} = \frac{i}{(4\pi)^2} \frac{(2\pi\mu)^{4-D}}{i\pi} \int d^D k \times \int_0^1 dx \frac{\partial^2}{\partial (m_j^2)^2} \frac{(1-x) N_{3\mu}(m_A, m_B)}{\Delta_\gamma \Delta_j(l) \Delta_B(p')} \Bigg|_{m_j=m_A}, \quad (13)$$

where $l = xp + (1-x)p'$ and $l' = yp + (1-y)p'$ have been defined. Keep in mind that the cases in which virtual-lepton flavor is conserved and changed are both comprehended by Eqs. (11)–(13). The regularization of loop integrals in these equations is carried out within the approach of dimensional regularization [48,66], in which case μ is a quantity with units $[\mu] = \text{mass}$ introduced to correct mass dimensions of amplitudes. In Eqs. (11)–(13), the factors $N_{j\mu} = N_{j\mu}(m_A, m_B)$, depending on charged-lepton masses and not affected by squared-mass derivatives, read

$$N_{1\mu} = -\frac{e^3 v^2}{4} \gamma^\nu (\not{k} + \not{p}' + m_A) (A_{\alpha\beta}^{BA*} \gamma_5 + V_{\alpha\beta}^{AB}) \times \sigma^{\alpha\beta} (\not{k} + \not{p}' + m_B) \gamma_\mu (\not{k} + \not{p}' + m_B) \times (A_{\rho\lambda}^{BA*} \gamma_5 + V_{\rho\lambda}^{AB}) \sigma^{\rho\lambda} (\not{k} + \not{p}' + m_A) \gamma_\nu, \quad (14)$$

$$N_{2\mu} = -\frac{e^3 v^2}{4} \gamma^\nu (\not{k} + \not{p}' + m_A) \gamma_\mu (\not{k} + \not{p}' + m_A) \times (A_{\alpha\beta}^{BA*} \gamma_5 + V_{\alpha\beta}^{AB}) \sigma^{\alpha\beta} (\not{k} + \not{p}' + m_B) \times (A_{\rho\lambda}^{BA*} \gamma_5 + V_{\rho\lambda}^{AB}) \sigma^{\rho\lambda} (\not{k} + \not{p}' + m_A) \gamma_\nu, \quad (15)$$

$$N_{3\mu} = -\frac{e^3 v^2}{4} \gamma^\nu (\not{k} + \not{p}' + m_A) (A_{\alpha\beta}^{BA*} \gamma_5 + V_{\alpha\beta}^{AB}) \times \sigma^{\alpha\beta} (\not{k} + \not{p}' + m_B) (A_{\rho\lambda}^{BA*} \gamma_5 + V_{\rho\lambda}^{AB}) \sigma^{\rho\lambda} \times (\not{k} + \not{p}' + m_A) \gamma_\mu (\not{k} + \not{p}' + m_A) \gamma_\nu. \quad (16)$$

We add all the individual loop-diagram analytic expressions to get the total contribution $\Gamma_\mu^A = \sum_{B=e,\mu,\tau} (\Gamma_{1\mu}^{AB} + \Gamma_{2\mu}^{AB} + \Gamma_{3\mu}^{AB})$. Through algebraic manipulations, we write this as

$$\Gamma_\mu^A = \frac{e}{2m_A} f_A^m \sigma_{\mu\nu} q^\nu + i f_A^d \sigma_{\mu\nu} q^\nu \gamma_5 + \dots, \quad (17)$$

where f_A^m and f_A^d are functions of field masses, squared photon momentum q^2 , and Lorentz-violating tensor coefficients $V_{\alpha\beta}^{AB}$ and $A_{\alpha\beta}^{AB}$. We emphasize that f_A^m and f_A^d , which from Eq. (1) are recognized as magnetic and electric form factors, respectively, are invariant under particle Lorentz

transformations. So, contributions to the AMM and to the EDM of the charged-lepton l_A can be straightforwardly extracted from such coefficients. The ellipsis in Eq. (17) represents a large set of terms, most of which involve violations of invariance under particle Lorentz transformations.

We define in the space of matrix representations of Lorentz transformations, the 4×4 matrices κ_1^{AB} , κ_2^{AB} , and κ_3^{AB} , with entries

$$(\kappa_1^{AB})_\alpha^\beta = V_{\alpha\nu}^{AB} V^{AB\nu\beta}, \quad (18)$$

$$(\kappa_2^{AB})_\alpha^\beta = A_{\alpha\nu}^{BA*} A^{BA\nu\beta*}, \quad (19)$$

$$(\kappa_3^{AB})_\alpha^\beta = V_{\alpha\nu}^{AB} A^{BA\nu\beta*}. \quad (20)$$

Since $A, B = e, \mu, \tau$, there are, in principle, 27 of these complex matrices, each of them bearing 32 parameters, thus yielding a grand total of 864 parameters, which, however, are not independent. In particular, the following relations hold: $(\kappa_1^{AB})_{\alpha\beta} = (\kappa_1^{AB})_{\beta\alpha}$ and $(\kappa_1^{AB})_{\alpha\beta} = (\kappa_1^{BA})_{\alpha\beta}^*$; $(\kappa_2^{AB})_{\alpha\beta} = (\kappa_2^{AB})_{\beta\alpha}$ and $(\kappa_2^{AB})_{\alpha\beta} = (\kappa_2^{BA})_{\alpha\beta}^*$; $(\kappa_3^{AB})_{\alpha\beta} = -(\kappa_3^{BA})_{\alpha\beta}^*$. As $(\kappa_j^{AB})_{\alpha\beta} = \pm(\kappa_j^{BA})_{\alpha\beta}^*$, for any fixed j , there are nine real matrices, say, $\text{Re}\{\kappa_j^{AB}\}$ and $\text{Im}\{\kappa_j^{AB}\}$, so the whole set of matrices comprises 27 elements with 16 real entries per matrix. Nonetheless, notice that in the cases $j = 1, 2$ a further reduction occurs due to symmetry in the space of matrix Lorentz representations. The numbers of parameters resulting from the complex quantities $(\kappa_j^{AB})_\alpha^\beta$, for each $j = 1, 2, 3$ and after taking these relations into account, are given in Table I, from which a total of 324 parameters are counted. However, the Lorentz-violating contributions to AMMs and EDMs under consideration do not carry information on all these parameters. A major reason motivating the definitions given in Eqs. (18)–(20) is that, as we show below, all Lorentz-violating contributions from the Yukawa sector to AMMs and EDMs emerge as linear combinations of traces $\text{tr}\kappa_j^{AB} = (\kappa_j^{AB})_\alpha^\alpha$, which are the SME quantities to be bounded.

The total contributions from the Lorentz-violating Yukawa sector, Eq. (3), to f_A -lepton magnetic and electric form factors f_A^m and f_A^d are expressed as

$$f_A^m = \hat{f}_A^m + \sum_{B \neq A} \tilde{f}_{AB}^m, \quad (21)$$

$$f_A^d = \hat{f}_A^d + \sum_{B \neq A} \tilde{f}_{AB}^d, \quad (22)$$

where \hat{f}_A^m and \hat{f}_A^d are virtual-lepton-flavor conserving, whereas \tilde{f}_{AB}^m and \tilde{f}_{AB}^d , with $A \neq B$, come from Feynman diagrams with virtual-lepton-flavor change. In terms of the kappa notation defined by Eqs. (18)–(20), we write

TABLE I. The number of parameters associated with Lorentz-violating factors $(\kappa_j^{AB})_\alpha^\beta$ for each $j = 1, 2, 3$. Keep in mind that coefficients $(\kappa_j^{AB})_\alpha^\beta$ are complex quantities, so the numbers shown in this table take into account both independent real and imaginary parts.

Parameters	$(\kappa_1^{AB})_\alpha^\beta$	$(\kappa_2^{AB})_\alpha^\beta$	$(\kappa_3^{AB})_\alpha^\beta$
Number	90	90	144

the magnetic- and electric-form-factor contributions from Feynman diagrams that preserve virtual-lepton flavor, that is $A = B$, as $\hat{f}_A^m = -\text{tr}\{\kappa_1^{AA} h_{a,1} + \kappa_2^{AA} h_{a,2}\}$ and $\hat{f}_A^d = -\text{tr}\{\kappa_3^{AA} h_{d,1}\}$, where the symbol “tr” denotes, as before, a trace operating on 4×4 matrices in the space of matrix representations of Lorentz transformations. The explicit expressions for the coefficients $h_{a,1}$, $h_{a,2}$, and $h_{d,1}$ are quite large and intricate functions of masses, with no practical use for the reader, so we have not included them in the present paper. UV divergences introduced by each contributing loop diagram lie exclusively within two-point scalar functions B_0 . Any such function can be expressed, after dimensional regularization, as $B_0 = \Delta_{\text{UV}} + (\text{finite terms})$, where $\Delta_{\text{UV}} = 1/(4-D) - \gamma_E + \log(4\pi/\mu^2)$ diverges as $D \rightarrow 4$ [67]. All B_0 functions share the same UV-divergent term Δ_{UV} , so any difference of the form $B_0^j - B_0^k$, with B_0^j and B_0^k denoting different two-point scalar functions, is free of UV divergences. We have been able to establish that all B_0 functions in both \hat{f}_A^m and \hat{f}_A^d appear in differences like this, so we conclude that every UV divergence is canceled from the contributions with $A = B$. In the next step, we perform derivatives with respect to squared masses, as indicated in Eqs. (11)–(13). Then, parametric integrals also shown in such equations are carried out, and the on-shell condition $q^2 \rightarrow 0$, which defines the AMM and EDM contributions, is implemented. The resulting virtual-lepton-flavor-conserving expressions are

$$\hat{a}_A^{f_A} = \frac{e^3 v^2}{4\pi^2 m_A^2} \text{tr} \left\{ -\kappa_1^{AA} \left(\Delta_{\text{IR}} + \log \frac{\mu^2}{m_A^2} \right) + \frac{3}{8} (\kappa_2^{AA} - 5\kappa_1^{AA}) \right\}, \quad (23)$$

$$\hat{d}_A^{f_A} = \frac{ie^3 v^2}{16\pi^2 m_A^3} \text{tr} \left\{ -2\kappa_3^{AA} \left(\Delta_{\text{IR}} + \log \frac{\mu^2}{m_A^2} \right) + 3\kappa_3^{AA} \right\}. \quad (24)$$

The already anticipated presence of IR divergences in the electromagnetic form factors is explicitly given by the factor $\Delta_{\text{IR}} + \log(\mu^2/m_A^2)$, so these quantities do not qualify as observables. Nevertheless, we previously discussed that such divergences are expected to vanish from some cross section. With this in mind, we aim at an estimation of the effects of the finite parts of these quantities on some

physical observable instead, for which we omit the divergent terms in what follows. For diagrams with virtual-lepton-flavor change, the same steps are followed. The corresponding contributions to AMMs are free of both

UV and IR divergences, whereas the resulting EDMs turn out to be IR divergent. Once such IR divergences have been removed, the virtual-lepton-flavor-changing contributions to AMMs and EDMs are expressed as

$$\begin{aligned} \tilde{a}_B^{f_A} = & \frac{e^3 v^2}{192\pi^2 m_A^6 (m_A^2 - m_B^2)^2} \text{tr} \left\{ (\kappa_1^{AB} - \kappa_2^{AB}) \left(34m_A^8 \log \frac{m_A^2}{m_B^2} + (m_A^2 - m_B^2) \left(-13m_A^4 m_B^2 + 18m_A^2 m_B^4 \right. \right. \right. \\ & + 2(-19m_A^4 m_B^2 + 11m_A^2 m_B^4 + 17m_A^6 - 9m_B^6) \log \frac{m_B^2}{m_B^2 - m_A^2} - 39m_A^6 \left. \left. \left. \right) + 24m_A^3 m_B (\kappa_1^{AB} + \kappa_2^{AB}) \right. \right. \\ & \left. \left. \left. \times \left(m_A^4 \log \frac{m_A^2}{m_B^2} + (m_A^2 - m_B^2) \left(2(m_A^2 - m_B^2) \log \frac{m_B^2}{m_B^2 - m_A^2} - m_A^2 \right) \right) \right) \right\}, \end{aligned} \quad (25)$$

$$\tilde{d}_B^{f_A} = \frac{ie^3 v^2 m_B^3}{4\pi^2 m_A^4 (m_A^2 - m_B^2)} \log \frac{m_B^2}{m_B^2 - m_A^2} \text{tr} \kappa_3^{AB}. \quad (26)$$

IV. ESTIMATION OF EFFECTS AND DISCUSSION

Known to exist since the realization of the Stern-Gerlach experiment [68] and the ulterior theoretical explanation provided by Uhlenbeck and Goudsmit [69,70], intrinsic magnetic moments of elementary particles, which gave birth to the concept of spin, receive quantum corrections dubbed AMMs [71]. In the cases of the electron and the muon, the corresponding SM predictions have been calculated and estimated with remarkable precision [72,73], whereas experimental studies have reached exceptional sensitivity [74–76]. The disparity among the SM contribution to the AMM of some fermion f , a_f^{SM} , and the current best experimental measurement a_f^{exp} is conventionally characterized by the quantity $\Delta a_f = a_f^{\text{exp}} - a_f^{\text{SM}}$. For the electron AMM,

$$\Delta a_e = -1.06(082) \times 10^{-12} \quad (27)$$

has been reported [72] and

$$\Delta a_\mu = 249(87) \times 10^{-11} \quad (28)$$

is the current value for the case of the muon [73]. These discrepancies being so tiny can be interpreted as suitable places to look for suppressed new physics beyond the SM. The much-less-known tau-lepton AMM was investigated by the authors of Ref. [77], who performed an analysis of collider data and then established the model-independent limits

$$-0.007 < a_\tau^{\text{NP}} < 0.005 \quad (29)$$

on new-physics contributions to this quantity.

While theoretically plausible and phenomenologically relevant, the EDMs of elementary particles have not been measured ever, so our best experimental knowledge on the

matter consists of bounds. Investigations of EDMs of elementary particles have found much motivation in their connection to the phenomenon of CP violation, an essential ingredient behind baryonic asymmetry [78]. Limits on the electron EDM d_e are particularly stringent. Experiments with thallium atoms and ytterbium fluoride molecules achieved high sensitivities, thus yielding upper bounds of order $10^{-27} e \cdot \text{cm}$ on $|d_e|$ [79–81]. Furthermore, the ACME Collaboration reported the improved upper limit [82]

$$|d_e| < 8.7 \times 10^{-29} e \cdot \text{cm} \quad (30)$$

at 90% C.L. The SM prediction lies about 15 orders of magnitude below current experimental sensitivity [83], thus rendering the search for new physics presumably originating EDMs a promising task. Three analyses aimed at the observation of the muon EDM were performed and reported in Ref. [84] by the Muon $g - 2$ Collaboration. This group concluded that the lack of any signal yields the bound [84]

$$|d_\mu| < 1.8 \times 10^{-19} e \cdot \text{cm} \quad (31)$$

at 95% C.L. An experimental investigation carried out by the Belle Collaboration searched for CP violation induced by the tau-lepton EDM, determining at 95% C.L. the limits [85]

$$-2.2 \times 10^{-17} e \cdot \text{cm} < \text{Re}(d_\tau) < 4.5 \times 10^{-17} e \cdot \text{cm}, \quad (32)$$

$$-2.5 \times 10^{-17} e \cdot \text{cm} < \text{Im}(d_\tau) < 0.8 \times 10^{-17} e \cdot \text{cm}. \quad (33)$$

An estimation of bounds on SME coefficients from the Yukawa sector given in Eq. (3) is the main objective of the present section. Being an effective field theory characterized by coefficients with Lorentz indices, this Lagrangian sector bears a large number of parameters. Aiming at the reduction of the number of such parameters, we consider scenarios defined by specific assumptions on Lorentz-nonconserving coefficients. This matter is addressed below in a concrete manner. Moreover, the implementation

of on-shell conditions on Eqs. (21) and (22) defines the MSME Yukawa leading contributions to AMMs as $f_A^m(q^2=0) = a_A^{\text{SME}}$, and EDMs as $f_A^d(q^2=0) = d_A^{\text{SME}}$. Then, using Eqs. (23)–(26), the resulting electromagnetic factors contributions can be rearranged as

$$a_A^{\text{SME}} = \sum_{j=1}^2 \sum_{B=e,\mu,\tau} a_j^{AB} \text{tr} \kappa_j^{AB}, \quad (34)$$

$$d_A^{\text{SME}} = \sum_{B=e,\mu,\tau} d_3^{AB} \text{tr} \kappa_3^{AB}, \quad (35)$$

which is convenient in order to determine bounds. Following Ref. [57], we assume that matrices $V_{\alpha\beta}$ and $A_{\alpha\beta}$ are symmetric in flavor space. Since these matrices are Hermitian and anti-Hermitian, respectively, $V_{\alpha\beta}$ are real and $A_{\alpha\beta}$ are imaginary. Therefore, according to Eqs. (18)–(20), traces $\text{tr} \kappa_1^{AB}$ and $\text{tr} \kappa_2^{AB}$ are real quantities, but $\text{tr} \kappa_3^{AB}$ is imaginary. Furthermore, these assumptions ensure that virtual-lepton-flavor-conserving contributions \hat{a}_A^{fA} and \hat{d}_A^{fA} given by Eqs. (23) and (24), respectively, are real.

Consider, in general, some sort of new physics generating contributions to magnetic and/or electric form factors of fermions. The resulting set of magnetic and electric form factors can be classified into [43,44] diagonal electromagnetic form factors, in which external fermions coincide with each other, and transition electromagnetic form factors characterized by different external fermions. If transitions connecting leptons to quarks are forbidden, each of these fermion types yields nine magnetic moments and nine electric moments, with each set arranged as a 3×3 matrix. All such matrices, whose diagonal entries are the diagonal moments and with the transition moments playing the roles of nondiagonal components, are conventionally assumed to be Hermitian, meaning that diagonal moments are real, whereas transition moments might be complex. Notice, however, that working with the vertex $A_\mu f_A f_A$ off shell may introduce thresholds, beyond which imaginary parts of diagonal moments might be induced. It turns out that, even though AMMs and EDMs are on-shell quantities, electromagnetic moments of unstable particles may have imaginary parts. This issue was addressed by the authors of Ref. [86], who asseverated that AMMs and EDMs are ensured to be real only as long as calculations are performed in the context of Lorentz-conserving quantum electrodynamics and suggested that *ad hoc* definitions of these electromagnetic properties should be given in more general situations. Their discussion included a two-loop calculation, which showed that even the SM produces complex AMMs and EDMs. The emergence of complex electromagnetic moments has been pointed out in Refs. [87,88] as well.

From the explicit expressions provided in Eqs. (25) and (26), notice that Lorentz-nonconserving contributions to charged-lepton AMMs and EDMs are complex, even

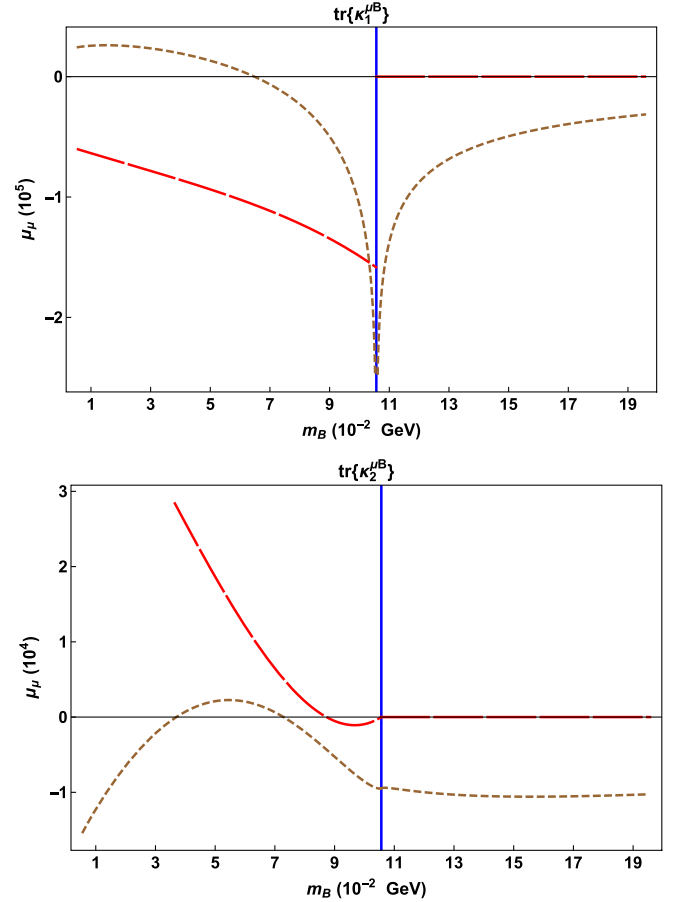


FIG. 3. Factors of traces in $a^{f,\mu}$, Eq. (34), as functions of the virtual-lepton mass m_B . The first graph displays $a_1^{\mu B}$, the coefficient of $\text{tr} \kappa_1^{\mu B}$, while $a_2^{\mu B}$, the coefficient of $\text{tr} \kappa_2^{\mu B}$, is shown in the second graph. Short-dashed plots stand for real parts of the factors, whereas long-dashed curves display imaginary parts of them. Vertical solid lines indicate where the threshold value $m_B = m_\mu$ lies.

though these electromagnetic moments are not transition-like, but diagonal moments instead, and even though they have been calculated on shell. In a general context, analogous imaginary parts of one-loop amplitudes, if present, usually emerge when some external field is connected to loop lines corresponding to particles which together are lighter than the external particle. In the case of the Lorentz-violating theory considered in the present investigation, the insertion of bilinear vertices connecting some external-field line to a lighter virtual-field line produces a like effect, which can be appreciated in Eqs. (25) and (26), where logarithmic factors $\log \frac{m_B^2}{m_B^2 - m_A^2}$ are real or imaginary depending on whether $m_B > m_A$ or $m_A > m_B$ holds. This is illustrated by the graphs in Figs. 3 and 4, which display the behavior of the real and imaginary parts of coefficients a_j^{AB} and d_3^{AB} defined by Eqs. (34) and (35), as functions of the virtual-lepton mass m_B for the case $A = \mu$ corresponding to external muons. The upper graph

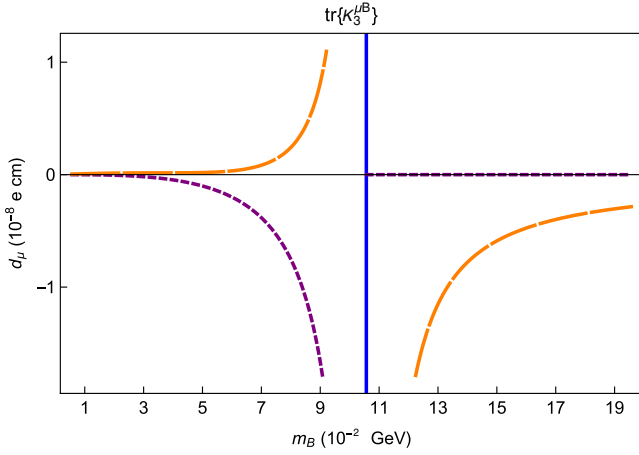


FIG. 4. Factors of traces in $d^{f\mu}$, Eq. (34), as functions of the virtual-lepton mass m_B . The first graph displays $d_3^{\mu B}$, the coefficient of $\text{tr}\kappa_3^{\mu B}$, while $d_4^{\mu B}$, the coefficient of $\text{tr}\kappa_4^{\mu B}$, is shown in the second graph, and $d_5^{\mu B}$, the coefficient of $\text{tr}\kappa_5^{\mu B}$, is depicted by the third graph. Short-dashed plots stand for real parts of the factors, whereas long-dashed curves display imaginary parts of them. Vertical solid lines indicate where the threshold value $m_B = m_\mu$ lies.

of Fig. 3 corresponds to $a_1^{\mu B}$, whereas the lower graph of this figure represents $a_2^{\mu B}$, both quantities being factors within the muon AMM contribution. In these graphs, short-dashed curves represent the real parts of coefficients $a_j^{\mu B}$, while long-dashed plots depict imaginary parts of such quantities. Moreover, horizontal solid lines represent the values $a_j^{\mu B} = 0$. Vertical solid lines located at value of the muon mass m_μ correspond to a m_B threshold, beyond which factors $a_j^{\mu B}$ are either complex or real quantities. Both graphs make it evident that the values of l_B mass such that $m_B < m_\mu$ yield imaginary-part contributions, but these contributions are real as long as $m_B > m_\mu$. Just as in Fig. 3, the short-dashed plot represents the real part of the factor $d_3^{\mu B}$ in the graph of Fig. 4, whereas the long-dashed curve is associated with its imaginary part. In this graph, the real part of $d_3^{\mu B}$ vanishes for $m_B > m_\mu$, but its imaginary part remains nonzero. This is correct, since the trace $\text{tr}\kappa_3^{\mu B}$ is purely imaginary, so a global imaginary factor from this trace should get things right. We have made sure that an analogous behavior occurs if external leptons f_τ are considered.

Now consider the 3×3 matrices

$$\mathcal{X}_j = \begin{pmatrix} \mathcal{X}_j^{ee} & \mathcal{X}_j^{e\mu} & \mathcal{X}_j^{e\tau} \\ \mathcal{X}_j^{\mu e} & \mathcal{X}_j^{\mu\mu} & \mathcal{X}_j^{\mu\tau} \\ \mathcal{X}_j^{\tau e} & \mathcal{X}_j^{\tau\mu} & \mathcal{X}_j^{\tau\tau} \end{pmatrix} \equiv \begin{pmatrix} \text{tr}\kappa_j^{ee} & \text{tr}\kappa_j^{e\mu} & \text{tr}\kappa_j^{e\tau} \\ \text{tr}\kappa_j^{\mu e} & \text{tr}\kappa_j^{\mu\mu} & \text{tr}\kappa_j^{\mu\tau} \\ \text{tr}\kappa_j^{\tau e} & \text{tr}\kappa_j^{\tau\mu} & \text{tr}\kappa_j^{\tau\tau} \end{pmatrix}. \quad (36)$$

Keep in mind that these matrices are not, by any means, related to transition electromagnetic moments, in which external fermions have different flavors. They exclusively correspond to diagonal electromagnetic moments, and rather characterize the terms of such quantities in which virtual-lepton flavor is preserved or changed. For instance, from Eq. (34), the contribution from Lorentz violation to the tau AMM is expressed as $a_\tau^{\text{SME}} = \sum_{j=1}^2 (a_j^{\tau e} \mathcal{X}_j^{\tau e} + a_j^{\tau\mu} \mathcal{X}_j^{\tau\mu} + a_j^{\tau\tau} \mathcal{X}_j^{\tau\tau})$. Then notice that the third rows of matrices \mathcal{X}_1 and \mathcal{X}_2 comprise all the SME traces $\mathcal{X}_j^{\tau B} = \text{tr}\kappa_j^{\tau B}$ necessary to determine this AMM contribution. In general, $\mathcal{X}_j^\dagger = \mathcal{X}_j$ holds for $j = 1, 2$, while $\mathcal{X}_3^\dagger = -\mathcal{X}_3$, so not all the traces defining the entries of matrices \mathcal{X}_j are independent. Moreover, our previous assumption that $V_{\alpha\beta}^{AB} = V_{\alpha\beta}^{BA}$ and $A_{\alpha\beta}^{AB} = A_{\alpha\beta}^{BA}$ ensures that \mathcal{X}_1 and \mathcal{X}_2 are symmetric and real, whereas \mathcal{X}_3 is symmetric and imaginary. Thus, each matrix \mathcal{X}_j is determined by six independent parameters \mathcal{X}_j^{AB} yielding a total of 18 independent parameters. Since AMM contributions are given exclusively in terms of \mathcal{X}_1 and \mathcal{X}_2 , these quantities are determined by 12 real traces, whereas EDMs expressed in terms of \mathcal{X}_3 involve six independent traces in total. With these definitions at hand, we now consider scenarios distinguished by textures of \mathcal{X}_j .

A. Quasidiagonal textures

The scenario of quasidiagonal textures is defined by the assumption that the diagonal entries of \mathcal{X}_j are by far dominant, whereas off-diagonal components of such matrices practically equal zero, namely, $\mathcal{X}_j^{AB} \approx 0$ for $A \neq B$. Then, \mathcal{X}_j matrices look like

$$\mathcal{X}_j \approx \begin{pmatrix} \mathcal{X}_j^e & 0 & 0 \\ 0 & \mathcal{X}_j^\mu & 0 \\ 0 & 0 & \mathcal{X}_j^\tau \end{pmatrix}, \quad (37)$$

where we have denoted $\mathcal{X}_j^{AA} = \mathcal{X}_j^A$. So, Eqs. (34) and (35) are expressed as

$$a_A^{\text{SME}} \approx a_1^{AA} \mathcal{X}_1^A + a_2^{AA} \mathcal{X}_2^A, \quad (38)$$

$$d_A^{\text{SME}} \approx d_3^{AA} \mathcal{X}_3^A, \quad (39)$$

where repeated flavor indices do not indicate sums.

As shown by Eq. (38), the assumption of quasidegenerate textures yields for each lepton flavor A a MSME contribution to AMM a_A^{SME} determined by only two parameters. We provide Figs. 5–7, which show parameter regions in $(\mathcal{X}_1^A, \mathcal{X}_2^A)$ spaces allowed by current constraints from beyond-SM physics on AMM given in Eqs. (27)–(29). Figure 5 displays the allowed region for the case of SME contributions to the electron AMM within

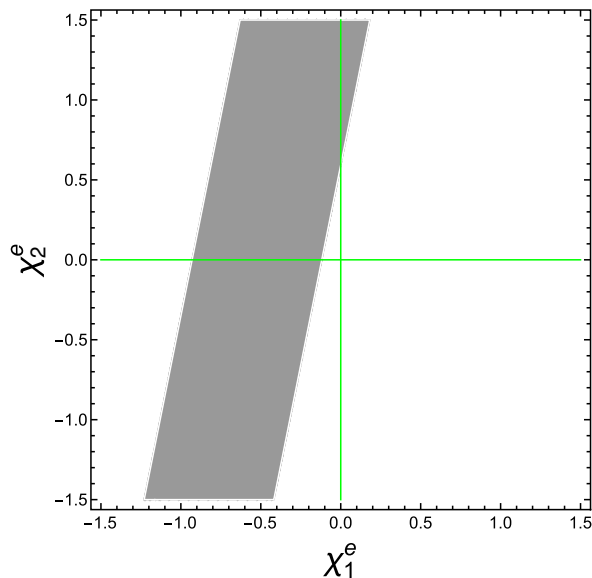


FIG. 5. For quasidegenerate texture, the allowed region within the parameter space $(\mathcal{X}_1^e, \mathcal{X}_2^e) \times 10^{21}$, for $|\mathcal{X}_1^e| < 1.5 \times 10^{-21}$ and $|\mathcal{X}_2^e| < 1.5 \times 10^{-21}$, in accordance with the AMM constraint displayed in Eq. (27).

$|\mathcal{X}_1^e| < 1.5 \times 10^{-21}$ and $|\mathcal{X}_2^e| < 1.5 \times 10^{-21}$. Aiming at a cleaner representation, the graph has been suitably rescaled by a factor of 10^{21} . An examination of this figure makes it clear that the Lorentz-violation coefficient \mathcal{X}_1^e is more restricted than \mathcal{X}_2^e . For any value of \mathcal{X}_2^e , the trace \mathcal{X}_1^e lies within a narrow interval of width $\approx 8.1 \times 10^{-22}$. Furthermore, as long as Lorentz-violation traces of order

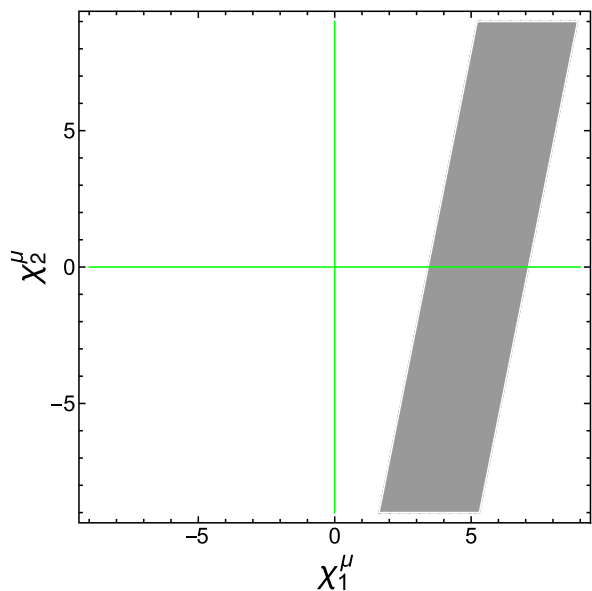


FIG. 6. For quasidegenerate texture, the allowed region within the parameter space $(\mathcal{X}_1^\mu, \mathcal{X}_2^\mu) \times 10^{14}$, for $|\mathcal{X}_1^\mu| < 9 \times 10^{-14}$ and $|\mathcal{X}_2^\mu| < 9 \times 10^{-14}$, in accordance with the AMM constraint displayed in Eq. (28).

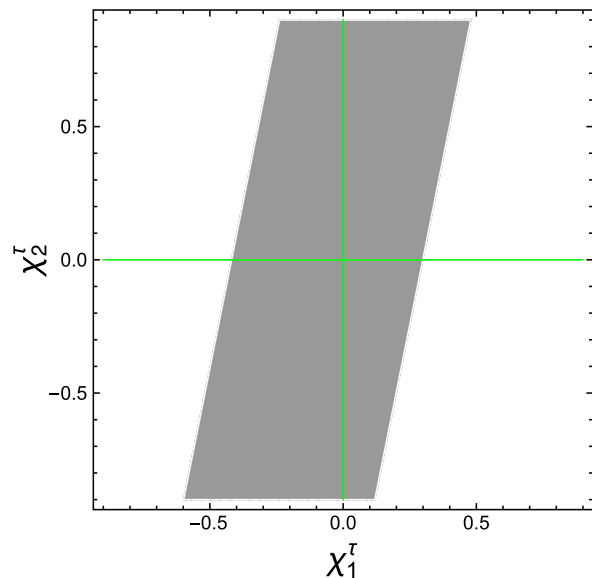


FIG. 7. For quasidegenerate texture, the allowed region within the parameter space $(\mathcal{X}_1^\tau, \mathcal{X}_2^\tau) \times 10^4$, for $|\mathcal{X}_1^\tau| < 1.5 \times 10^{-4}$ and $|\mathcal{X}_2^\tau| < 1.5 \times 10^{-4}$, in accordance with the AMM constraint displayed in Eq. (29).

$\lesssim 10^{-21}$ are assumed, the value of \mathcal{X}_1^e is more likely to be negative. Similar explanations for Figs. 6 and 7 apply, but with the corresponding graphs rescaled by factors of 10^{14} and 10^4 , respectively. From Fig. 6, $\mathcal{X}_1^\mu > 0$ if muon-flavor traces of Lorentz-violating matrices are of order $\lesssim 10^{-14}$. To better illustrate the values of the parameters \mathcal{X}_1^A and \mathcal{X}_2^A considered for the realization of Figs. 5–7, we refer the reader to Table II which carries data for lepton flavors $A = e, \mu, \tau$. The first rows of these tables display the minimum (“bottom” column) and maximum (“top” column) \mathcal{X}_2^A values considered for the graphs of Figs. 5–7. The same rows include intervals of \mathcal{X}_1^A values within the allowed regions in the graphs determined by the fixed upper and lower values of parameters \mathcal{X}_2^A .

The determination of the bounds in the case of lepton EDMs is simpler. From Eq. (39), each new-physics contribution d_A^{SME} is expressed in terms of only one trace if

TABLE II. Values of Lorentz-violation parameters \mathcal{X}_1^A and \mathcal{X}_2^A , with $A = e, \mu, \tau$ from lepton AMMs constraints. Fixed parameters \mathcal{X}_j^A , in each row correspond to either the bottom (second column) or top (third column) values of a graph in Figs. 5–7.

	Bottom	Top
\mathcal{X}_2^e fixed	-15×10^{-22}	$+15 \times 10^{-22}$
$\Rightarrow \mathcal{X}_1^e$	$-8.25(405) \times 10^{-22}$	$-2.25(405) \times 10^{-22}$
\mathcal{X}_2^μ fixed	-9×10^{-14}	$+9 \times 10^{-14}$
$\Rightarrow \mathcal{X}_1^\mu$	$3.46(184) \times 10^{-14}$	$7.06(184) \times 10^{-14}$
\mathcal{X}_2^τ fixed	-9×10^{-5}	$+9 \times 10^{-5}$
$\Rightarrow \mathcal{X}_1^\tau$	$-2.39(358) \times 10^{-5}$	$1.20(358) \times 10^{-5}$

quasidegenerate textures are assumed. From the current limits on lepton EDMs displayed in Eqs. (30)–(32), the following bounds are derived:

$$|\chi_3^e| < 5.58 \times 10^{-27}, \quad (40)$$

$$|\chi_3^\mu| < 1.02 \times 10^{-10}, \quad (41)$$

$$-5.95 \times 10^{-5} < -i\chi_3^\tau < 1.21 \times 10^{-4}. \quad (42)$$

B. Hermitian matrices $Y_{\alpha\beta}$

Consider a scenario in which $Y_{\alpha\beta}^\dagger = Y_{\alpha\beta}$ holds. As previously pointed out, this assumption yields, according to Eqs. (4) and (5), an exact cancellation of Lorentz-violating coefficients $A_{\alpha\beta}^{AB}$ while leaving nonzero factors $V_{\alpha\beta}^{AB}$. Under such circumstances, only the matrix \mathcal{X}_1 remains nonzero, so the whole set of AMM contributions is written in terms of six \mathcal{X}_1 parameters, whereas no contributions to EDMs exist. To discuss the AMM contributions, we define the factors

$$\Delta_1^H = \frac{\mathcal{X}_1^{e\mu}}{\mathcal{X}_1^{\tau e}}, \quad \Delta_2^H = \frac{\mathcal{X}_1^{\tau e}}{\mathcal{X}_1^{\mu\tau}} \quad (43)$$

in terms of which the new-physics contributions are written as

$$a_e^{\text{SME}} = a_1^{ee} \mathcal{X}_1^e + \Delta_2^H (a_1^{e\mu} \Delta_1^H + a_1^{e\tau}) \mathcal{X}_1^{\mu\tau}, \quad (44)$$

$$a_\mu^{\text{SME}} = a_1^{\mu\mu} \mathcal{X}_1^\mu + (a_1^{\mu e} \Delta_1^H \Delta_2^H + a_1^{\mu\tau}) \mathcal{X}_1^{\mu\tau}, \quad (45)$$

$$a_\tau^{\text{SME}} = a_1^{\tau\tau} \mathcal{X}_1^\tau + (a_1^{\tau e} \Delta_2^H + a_1^{\tau\mu}) \mathcal{X}_1^{\mu\tau}. \quad (46)$$

In this manner, each contribution corresponding to any lepton flavor A is expressed in terms of four parameters. For any flavor A , three such quantities are the factors Δ_1^H , Δ_2^H , and the trace $\mathcal{X}_1^{\mu\tau}$, while the parameter \mathcal{X}_1^A , which is the only one distinguishing the specific A -flavor contribution, defines the expression as well. The fact that Eqs. (44)–(46) share three Lorentz-violation parameters is a feature to bear in mind, for the contributions a_e^{SME} , a_μ^{SME} , a_τ^{SME} are in part simultaneously determined by such parameters. To provide a qualitative description of the SME contributions a_A^{SME} in this scenario, the graphs of Figs. 8–11 have been plotted.

The two graphs of Fig. 8 displaying the allowed regions in the space of parameters $(\mathcal{X}_1^e, \mathcal{X}_1^{\mu\tau})$ and determined by the bounds on contributions from new physics to the electron AMM, Eq. (27), have been realized within $|\mathcal{X}_1^e| < 1.5$ and $|\mathcal{X}_1^{\mu\tau}| < 5$ after a proper rescaling by the factor 10^{21} . Two graphs have been included in order to compare the allowed regions for scenarios characterized by different choices of the parameter Δ_1^H . The values $\Delta_1^H = 10$ in the upper graph and $\Delta_1^H = 10^2$ in the lower graph have been considered,

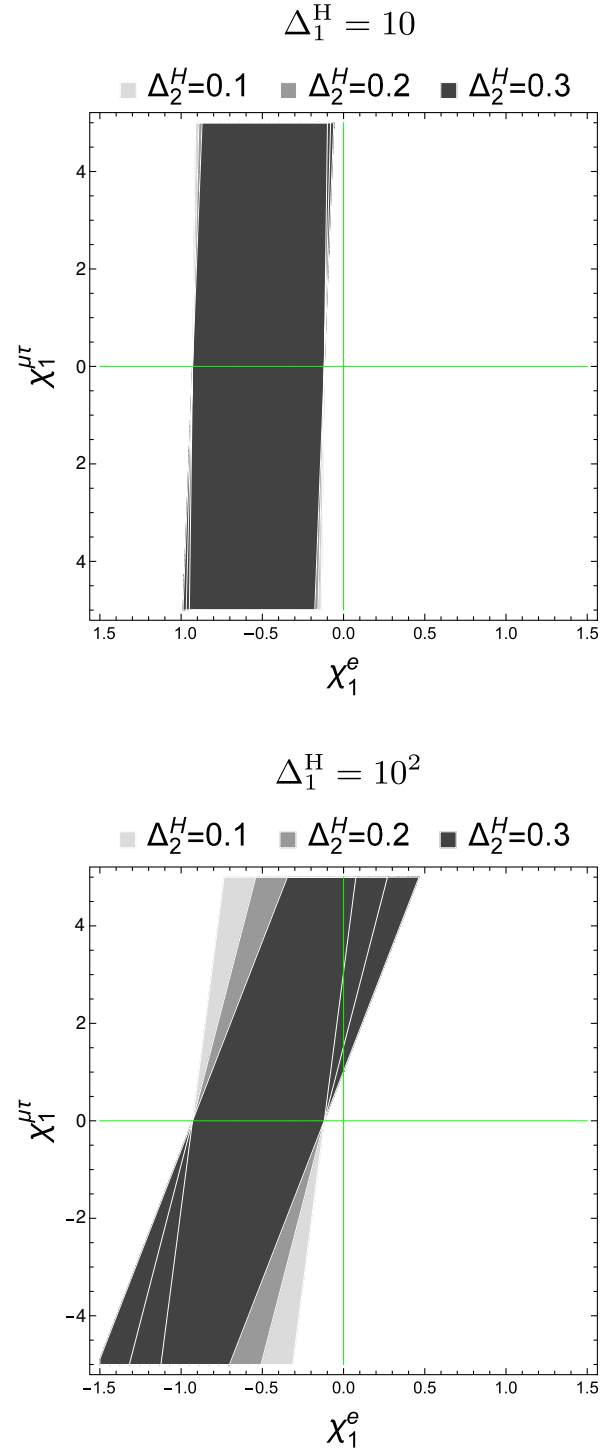


FIG. 8. Allowed regions in the parameter space $(\mathcal{X}_1^e, \mathcal{X}_1^{\mu\tau})$, within $|\mathcal{X}_1^e| < 1.5 \times 10^{-26}$ and $|\mathcal{X}_1^{\mu\tau}| < 5 \times 10^{-26}$, with both graphs rescaled by 10^{26} . We consider values $\Delta_1^H = 10$ (upper graph) and $\Delta_1^H = 10^2$ (lower graph), whereas $\Delta_2^H = 0.1, 0.2, 0.3$ are used in both cases.

whereas for each graph the values $\Delta_2^H = 0.1, 0.2, 0.3$ have been taken into account. The three allowed regions shown by each graph are straight strips whose widths are similar to

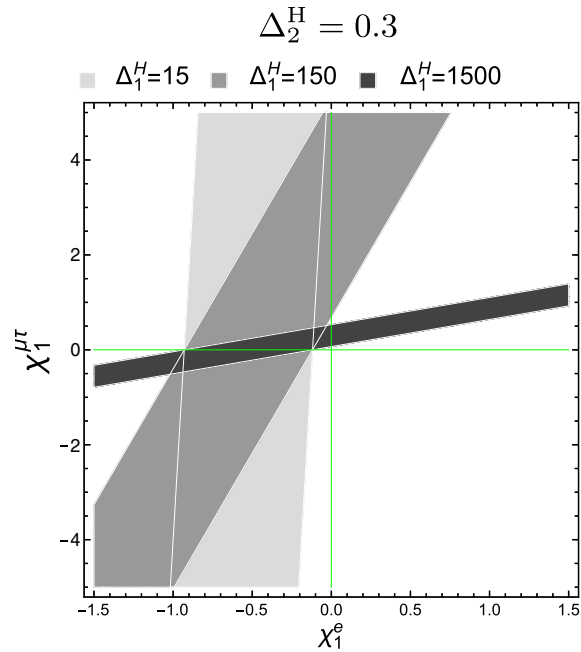
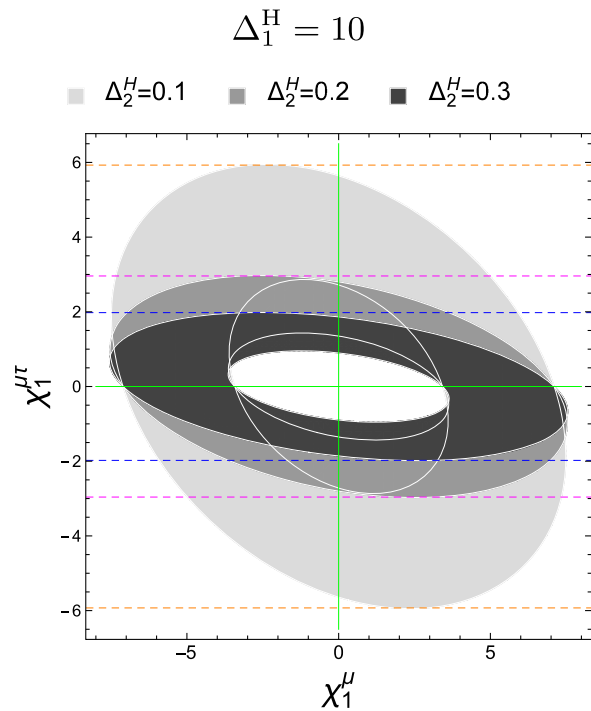


FIG. 9. Allowed regions in the parameter space $(\chi_1^e, \chi_1^{\mu\tau})$, within $|\chi_1^e| < 1.5 \times 10^{-26}$ and $|\chi_1^{\mu\tau}| < 5 \times 10^{-26}$, with the graph rescaled by 10^{26} . We consider values $\Delta_1^H = 15, 150, 1500$, whereas $\Delta_2^H = 0.3$ is taken.

each other for each considered Δ_2^H value. In the case $\Delta_1^H = 10$, the allowed regions are barely distinguished from each other, whereas the shapes of the regions seem to be more sensitive to changes in Δ_2^H as long as the value $\Delta_1^H = 10^2$, larger by 1 order of magnitude, is considered. These graphs illustrate how orientations of allowed regions are, in general, different for different values of Δ_2^H with fixed Δ_1^H . In this context, the SME trace χ_1^e is more stringently constrained than $\chi_1^{\mu\tau}$ in both scenarios. Nonetheless, the last statement realized for particular choices of factors Δ_1^H and Δ_2^H should not be understood to be valid in general. To illustrate this, we provide Fig. 9, which has been realized within the same parameter region $(\chi_1^e, \chi_1^{\mu\tau})$ as that of the graphs of Fig. 8, and with the same rescaling as well. In this case, the values $\Delta_2^H = 0.3$ and $\Delta_1^H = 15, 150, 1500$ have been utilized. Then notice that the largest value of Δ_1^H , among those considered for the realization of this graph, yields an allowed-region strip which, in comparison with the allowed regions of Fig. 8, is narrower with a clockwise-rotated orientation, thus corresponding to a parameter $\chi_1^{\mu\tau}$ more stringently restricted than χ_1^e , as opposite to the allowed regions of Fig. 8.

Regarding the contributions from the SME to the AMM of the muon, the graphs of Fig. 10 provide a depiction of the allowed regions in the parameter space $(\chi_1^\mu, \chi_1^{\mu\tau})$, with a



$$\Delta_1^H = 10^2$$

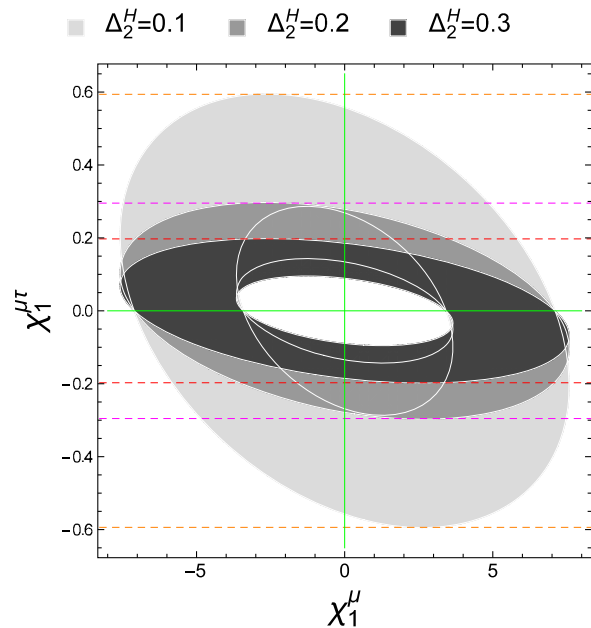


FIG. 10. Allowed regions in the parameter space $(\chi_1^\mu, \chi_1^{\mu\tau})$, within $|\chi_1^\mu| < 8 \times 10^{-14}$ and either $|\chi_1^{\mu\tau}| < 6 \times 10^{-14}$ (upper graph) or $|\chi_1^{\mu\tau}| < 0.6 \times 10^{-14}$ (lower graph), with both graphs rescaled by 10^{14} . We consider values $\Delta_1^H = 10$ (upper graph) and $\Delta_1^H = 10^2$ (lower graph), whereas $\Delta_2^H = 0.1, 0.2, 0.3$ are used in both cases. Pairs of dashed horizontal lines define $\chi_1^{\mu\tau}$ -allowed intervals around $\chi_1^{\mu\tau} = 0$.

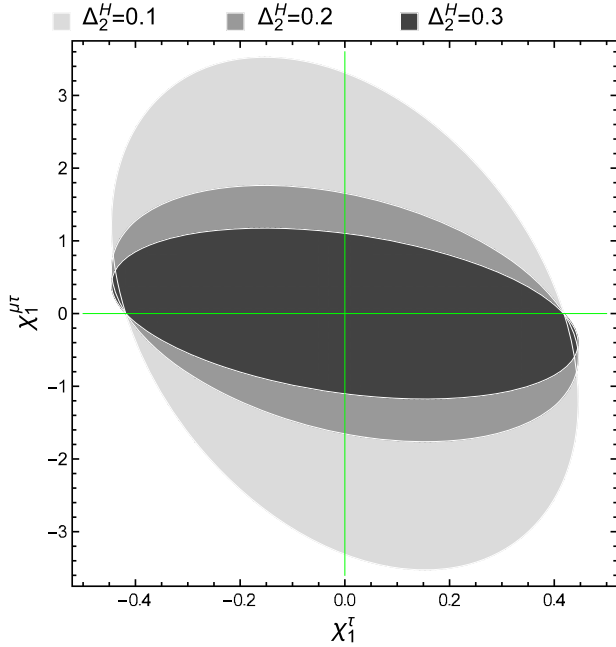


FIG. 11. Allowed regions in the parameter space $(\mathcal{X}_1^\tau, \mathcal{X}_1^{\mu\tau})$, within $|\mathcal{X}_1^\tau| < 0.35 \times 10^{-4}$ and $|\mathcal{X}_1^{\mu\tau}| < 2.6 \times 10^{-4}$, with the graph rescaled by 10^4 . We consider values $\Delta_2^H = 0.1, 0.2, 0.3$, for any Δ_1^H .

convenient rescaling by a factor 10^{14} implemented in the two graphs. In the present scenario, the contribution a_μ^{SME} is complex valued, so its modulus, $|a_\mu^{\text{SME}}|$ has been rather considered to compare it with the bound from new physics on the muon AMM, Eq. (28), which corresponds to an interval of positive values. Thus, the allowed regions shown in Fig. 10 are not straight strips, but rings instead. The values of the factors Δ_1^H and Δ_2^H utilized to plot the graphs of Fig. 10 are the same as those of Fig. 8; that is, $\Delta_1^H = 10$ and $\Delta_1^H = 10^2$, respectively, were used to plot the upper graph and the lower graph of Fig. 10, whereas the values $\Delta_2^H = 0.1, 0.2, 0.3$ were all considered in both graphs. With this in mind, notice that for fixed Δ_1^H , increasing the values of the parameter Δ_2^H flattens the ring along the $\mathcal{X}_1^{\mu\tau}$ axis, in which case larger values of Δ_2^H correspond to more restricted allowed regions. While values within $|\mathcal{X}_1^\mu| < 8 \times 10^{-14}$ have been considered for both graphs, vertical axes range along different intervals: The upper-graph vertical axis runs over $|\mathcal{X}_1^{\mu\tau}| < 6 \times 10^{-14}$; the lower graph, on the other hand, displays values of the vertical axis within $|\mathcal{X}_1^{\mu\tau}| < 0.6 \times 10^{-14}$. So, notice that the choice $\Delta_1^H = 10^2$ for the lower graph yields more constrained regions than those corresponding to $\Delta_1^H = 10$.

Next we focus on the SME contributions to the tau AMM, which we illustrate by means of Fig. 11. This figure displays one sole graph plotted within $|\mathcal{X}_1^\tau| < 0.35 \times 10^{-4}$ and $|\mathcal{X}_1^{\mu\tau}| < 2.6 \times 10^{-4}$, and normalized by the factor 10^4 . Notice from Eq. (46) that a_τ^{SME} is Δ_1^H independent, so there

TABLE III. Allowed intervals of $\mathcal{X}_1^{\mu\tau}$ values for different choices of parameters Δ_1^H and Δ_2^H and determined from lepton AMMs bounds on new-physics effects, implemented on the MSME Yukawa-sector contributions a_A^{SME} in the scenario of Hermitian matrices $Y_{\alpha\beta}$.

	Δ_1^H	Δ_2^H	$ \mathcal{X}_1^{\mu\tau} <$
a_A^{SME}	10	0.1	5.93×10^{-14}
	10	0.2	2.96×10^{-14}
	10	0.3	1.98×10^{-14}
	10^2	0.1	0.59×10^{-14}
	10^2	0.2	0.29×10^{-14}
	10^2	0.3	0.19×10^{-14}

is no need to include more graphs to compare regions associated with different values of the factor Δ_1^H . As it occurred in the case $A = \mu$, previously discussed, the SME contribution a_τ^{SME} to the tau AMM is a complex-valued quantity. Thus, the modulus $|a_\tau^{\text{SME}}|$ was considered, and since the bounds on this AMM define an interval which includes both positive and negative values, the resulting allowed regions do not involve holes. Again, the plotted allowed regions correspond to the values $\Delta_2^H = 0.1, 0.2, 0.3$. This graph shows that the larger the value of Δ_2^H , the flattest the ellipse along the $\mathcal{X}_1^{\mu\tau}$ axis and, thus, the smaller the allowed region in the parameter space $(\mathcal{X}_1^\tau, \mathcal{X}_1^{\mu\tau})$.

Among the three MSME AMM contributions, the most stringent constraints on $\mathcal{X}_1^{\mu\tau}$ of orders 10^{-15} to 10^{-14} are set by $|a_\mu^{\text{SME}}|$. The corresponding allowed intervals are displayed in the graphs of Fig. 10 through pairs of horizontal dashed lines which are equidistant from the horizontal axes. Each graph then shows three such intervals. The precise numerical values of these limits are given in the fourth column of Table III.

V. SUMMARY

The present investigation has been performed in the context established by the Lorentz- and *CPT*-violating Standard Model extension, an effective field theory which sets a quite general framework to quantify, at relatively low energies, the effects to be expected from a higher-energy formulation incorporating violation of Lorentz invariance. While this model of new physics extends every sector of the Standard Model, by the inclusion of both renormalizable and nonrenormalizable Lagrangian terms, our discussion has been restricted to couplings occurring in the Yukawa sector of the renormalizable part of the Standard Model extension. This sort of Lorentz nonconservation is characterized by Yukawa-like couplings endowed with spacetime Lorentz indices, which come along with noninvariance under particle transformations, even though observer transformations remain a symmetry of the theory.

TABLE IV. Bounds on SME coefficients from the Lorentz-violating Yukawa sector.

Assumptions	EMMs	Combinations	Bounds
QDT, $\text{tr}\kappa_2^{ee} = \pm 1.5 \times 10^{-21}$	a_e^{SME}	$\text{tr}\kappa_1^{ee}$	$-2.25(405) \times 10^{-22}$ $-8.25(405) \times 10^{-22}$
QDT, $\text{tr}\kappa_2^{\mu\mu} = \pm 5.0 \times 10^{-10}$	a_μ^{SME}	$\text{tr}\kappa_1^{\mu\mu}$	$+7.06(184) \times 10^{-14}$ $+3.46(184) \times 10^{-14}$
QDT, $\text{tr}\kappa_2^{\tau\tau} = \pm 9.0 \times 10^{-5}$	a_τ^{SME}	$\text{tr}\kappa_1^{\tau\tau}$	$+1.20(358) \times 10^{-5}$ $-2.39(358) \times 10^{-5}$
QDT	d_e^{SME}	$ \text{tr}\kappa_3^{ee} $	$< 5.58 \times 10^{-27}$
QDT	d_μ^{SME}	$ \text{tr}\kappa_3^{\mu\mu} $	$< 1.02 \times 10^{-10}$
QDT	d_τ^{SME}	$-i\text{tr}\kappa_3^{ee}$	$> -5.95 \times 10^{-5}$ $< 1.21 \times 10^{-4}$
HYM, $\Delta_1^H = 10$, $\Delta_2^H = 0.3$	$ a_\mu^{\text{SME}} $	$ \text{tr}\kappa_1^{\mu\tau} $	$< 1.98 \times 10^{-14}$
HYM, $\Delta_1^H = 10^2$, $\Delta_2^H = 0.3$	$ a_\mu^{\text{SME}} $	$ \text{tr}\kappa_1^{\mu\tau} $	$< 0.19 \times 10^{-14}$

In a perturbative approach, the Lorentz-violating interactions resulting from this extended Yukawa sector, after implementation of the Brout-Englert-Higgs mechanism, yield two-point insertions and three-point vertices which induce one-loop corrections to the electromagnetic vertex $A_\mu l_A l_A$. In the presence of Lorentz nonpreservation, $A_\mu l_A l_A$ is characterized by a tensor structure with several form factors adding to those already known to define the ordinary Lorentz-invariant parametrization of such interactions. In this context, the aforementioned loop corrections involve contributions to both magnetic and electric form factors. For these quantities to consistently be Lorentz invariant, the contributions from this new physics have been argued to emerge for the first time at the second order in Lorentz-violating coefficients. With this in mind, leading contributions from Lorentz violation to anomalous magnetic moments and electric dipole moments have been identified, with the corresponding expressions being quantified by flavor-mixing coefficients $\text{tr}\kappa_1^{AB} = V_{\nu\alpha}^{AB} V_{\nu\alpha}^{AB}$, $\text{tr}\kappa_2^{AB} = A_{\nu\alpha}^{BA*} A_{\nu\alpha}^{BA}$, and $\text{tr}\kappa_3^{AB} = V_{\nu\alpha}^{AB} A_{\nu\alpha}^{BA}$. The resulting contributions from Lorentz-violation to anomalous magnetic moments and electric dipole moments have been found to be ultraviolet finite. Nonetheless, the contributions bear infrared divergences that cannot be removed from amplitudes, so these electromagnetic moments contributions are not measurable. Even so, since such divergences are expected to vanish at the cross-section level, the infrared-divergent terms have been removed from the contributions in order to estimate the impact of these interactions on some physical process. Imaginary parts of the muon and tau-lepton electromagnetic moments emerge, even though the calculation has been carried out on shell and has included only diagonal moments. This happens in the perturbative approach, followed here, because bilinear insertions allow for Feynman diagrams in which external lines connect to virtual lines associated with lighter particles, thus defining thresholds which are surpassed by the contributions after on-shell conditions are implemented.

Defining 3×3 matrices \mathcal{X}_j with lepton-flavor components $\mathcal{X}_j^{AB} = \text{tr}\kappa_j^{AB}$, where $j = 1, 2, 3$ and where the trace tr operates on 4×4 matrices κ_j^{AB} given in the space of matrix representations of the Lorentz group, we have considered and explored two scenarios. One of them, which we have named ‘‘scenario of quasideagonal textures,’’ is defined by the conditions $\mathcal{X}_j^{AB} \approx 0$ for $A \neq B$. In this context, each electromagnetic moment is determined by Lorentz-violation parameters not shared by any other moment, so the comparison between each electromagnetic moment contribution and its corresponding bound, as taken from the literature, has been carried out independently of any other contribution. Moreover, in this scenario all the contributions from Lorentz violation are real. A summary of the bounds determined in this scenario is provided in Table IV, where constraints derived within this scenario can be found in rows including the assumption ‘‘QDT,’’ which is an acronym for quasideagonal textures. From this table, note that the most stringent bounds restricting SME coefficients $\text{tr}\kappa_j^{ee}$ are established by the electron EDM, whereas the most stringent bound given by AMMs limits on new-physics effects of order 10^{-22} also correspond to the case of the electron. As expected, for both electromagnetic moment Lorentz-violation contributions, the weakest constraints are determined by the restrictions on the tau-lepton electromagnetic moments. A scenario of Hermitian Yukawa matrices, which in Table IV has been referred to by the acronym ‘‘HYM,’’ is defined by the condition $Y_{\mu\nu}^\dagger = Y_{\mu\nu}$, which yields the exact cancellation of coefficients $A_{\mu\nu}^{BA*}$, so no contributions to electric dipole moments are generated. In this scenario, the Lorentz-violation contributions to the anomalous magnetic moments of the muon and the tau lepton, which are unstable particles, have turned out to be complex quantities. The comparison of SME contributions with current bounds on such electromagnetic moments and the corresponding analysis is more intricate than the one executed in the other scenario, the reason being that all the anomalous-magnetic-moment

contributions share SME parameters, together with the fact that bounds on these quantities are quite different from each other. Under such circumstances, the parameter $|\text{tr } \kappa_1^{\mu\nu}|$ is the one which has been bounded. The most restrictive limits constraining $|\text{tr } \kappa_1^{\mu\nu}|$ are as stringent as 10^{-15} .

ACKNOWLEDGMENTS

The authors acknowledge financial support from Consejo Nacional de Ciencia y Tecnología and Sistema Nacional de Investigadores (México). J.M. thanks Cátedras Conacyt Project No. 1753.

-
- [1] S.L. Glashow, Partial-symmetries of weak interactions, *Nucl. Phys.* **22**, 579 (1961).
- [2] A. Salam, Weak and electromagnetic interactions, *Conf. Proc.* **C680519**, 367 (1968).
- [3] S. Weinberg, A Model of Leptons, *Phys. Rev. Lett.* **19**, 1264 (1967).
- [4] M. Tanabashi *et al.* (Particle Data Group), Review of particle physics, *Phys. Rev. D* **98**, 030001 (2018).
- [5] J. Wudka, Electroweak effective Lagrangians, *Int. J. Mod. Phys. A* **09**, 2301 (1994).
- [6] V. A. Kostelecký and S. Samuel, Spontaneous breaking of Lorentz symmetry in string theory, *Phys. Rev. D* **39**, 683 (1989).
- [7] V. A. Kostelecký and R. Potting, *CPT* and strings, *Nucl. Phys.* **B359**, 545 (1991).
- [8] V. A. Kostelecký and R. Potting, *CPT*, strings, and meson factories, *Phys. Rev. D* **51**, 3923 (1995).
- [9] S. M. Carroll, J. A. Harvey, V. A. Kostelecký, C. D. Lane, and T. Okamoto, Noncommutative Field Theory and Lorentz Violation, *Phys. Rev. Lett.* **87**, 141601 (2001).
- [10] V. A. Kostelecký and N. Russell, Data tables for Lorentz and *CPT* violation, *Rev. Mod. Phys.* **83**, 11 (2011).
- [11] A. Dobado, A. Gómez-Nicola, A. L. Maroto, and J. R. Peláez, *Effective Lagrangians for the Standard Model* (Springer-Verlag, Berlin, 1997).
- [12] D. Colladay and V. A. Kostelecký, *CPT* violation and the standard model, *Phys. Rev. D* **55**, 6760 (1997).
- [13] D. Colladay and V. A. Kostelecký, Lorentz-violating extension of the standard model, *Phys. Rev. D* **58**, 116002 (1998).
- [14] J. D. Tasson, What do we know about Lorentz invariance?, *Rep. Prog. Phys.* **77**, 062901 (2014).
- [15] V. A. Kostelecký and M. Mewes, Signals for Lorentz violation in electrodynamics, *Phys. Rev. D* **66**, 056005 (2002).
- [16] V. A. Kostelecký and M. Mewes, Electrodynamics with Lorentz-violating operators of arbitrary dimension, *Phys. Rev. D* **80**, 015020 (2009).
- [17] R. Lehnert and R. Potting, Vacuum Čerenkov Radiation, *Phys. Rev. Lett.* **93**, 110402 (2004).
- [18] R. Lehnert and R. Potting, Čerenkov effect in Lorentz-violating vacua, *Phys. Rev. D* **70**, 125010 (2004).
- [19] B. Altschul, Vacuum Čerenkov Radiation in Lorentz-Violating Theories Without *CPT* Violation, *Phys. Rev. Lett.* **98**, 041603 (2007).
- [20] B. Altschul, Čerenkov radiation in a Lorentz-violating and birefringent vacuum, *Phys. Rev. D* **75**, 105003 (2007).
- [21] B. Altschul, Finite duration and energy effects in Lorentz-violating vacuum Čerenkov radiation, *Nucl. Phys.* **B796**, 262 (2008).
- [22] B. Altschul, Absence of long-wavelength Čerenkov radiation with isotropic Lorentz and *CPT* violation, *Phys. Rev. D* **90**, 021701 (2014).
- [23] V. A. Kostelecký and M. Mewes, Lorentz and *CPT* violation in the neutrino sector, *Phys. Rev. D* **70**, 031902 (2004).
- [24] V. A. Kostelecký and M. Mewes, Lorentz and *CPT* violation in neutrinos, *Phys. Rev. D* **69**, 016005 (2004).
- [25] J. S. Díaz and V. A. Kostelecký, Lorentz- and *CPT*-violating models for neutrino oscillations, *Phys. Rev. D* **85**, 016013 (2012).
- [26] J. S. Díaz, T. Katori, J. Spitz, and J. M. Conrad, Search for neutrino-antineutrino oscillations with a reactor experiment, *Phys. Lett. B* **727**, 412 (2013).
- [27] A. Moyotl, H. Novales-Sánchez, J. J. Toscano, and E. S. Tututi, Gauge invariant electromagnetic properties of fermions induced by *CPT*-violation in the Standard Model extension, *Int. J. Mod. Phys. A* **29**, 1450039 (2014).
- [28] A. Moyotl, H. Novales-Sánchez, J. J. Toscano, and E. S. Tututi, One-loop nonbirefringent effects on the electromagnetic vertex in the Standard Model Extension, *Int. J. Mod. Phys. A* **29**, 1450107 (2014).
- [29] V. A. Kostelecký, C. D. Lane, and A. G. M. Pickering, One-loop renormalization of Lorentz-violating electrodynamics, *Phys. Rev. D* **65**, 056006 (2002).
- [30] J. Castro-Medina, H. Novales-Sánchez, J. J. Toscano, and E. S. Tututi, Decays $Z \rightarrow \gamma\gamma$ and $Z \rightarrow gg$ in the Standard Model extension, *Int. J. Mod. Phys. A* **30**, 1550216 (2015).
- [31] V. A. Kostelecký and M. Mewes, Neutrinos with Lorentz-violating operators of arbitrary dimension, *Phys. Rev. D* **85**, 096005 (2012).
- [32] V. A. Kostelecký and M. Mewes, Fermions with Lorentz-violating operators of arbitrary dimension, *Phys. Rev. D* **88**, 096006 (2013).
- [33] T. Mariz, J. R. Nascimento, A. Yu Petrov, and H. Belich, On one-loop corrections in the non-minimal dimension-five extension of QED, *J. Phys. Commun.* **1**, 045011 (2017).
- [34] R. Casaca, M. M. Ferreira, Jr., L. Lisboa-Santos, F. E. P. dos Santos, and M. Schreck, Maxwell electrodynamics modified by *CPT*-even and Lorentz-violating dimension-6 higher-derivative terms, *Phys. Rev. D* **97**, 115043 (2018).
- [35] M. M. Ferreira, Jr., L. Lisboa-Santos, R. V. Maluf, and M. Schreck, Maxwell electrodynamics modified by a *CPT*-odd dimension-five higher-derivative term, *Phys. Rev. D* **100**, 055036 (2019).

- [36] W. F. Chen and G. Kunstatter, Constraint from the Lamb shift and anomalous magnetic moment on radiatively induced Lorentz and CPT violation in quantum electrodynamics, *Phys. Rev. D* **62**, 105029 (2000).
- [37] C. D. Carone, M. Sher, and M. Vanderhaeghen, New bounds on isotropic Lorentz violation, *Phys. Rev. D* **74**, 077901 (2006).
- [38] J. B. Araujo, R. Casana, and M. M. Ferreira, Jr., Constraining CPT -even and Lorentz-violating nonminimal couplings with the electron magnetic and electric dipole moments, *Phys. Rev. D* **92**, 025049 (2015).
- [39] J. B. Araujo, R. Casana, and M. M. Ferreira, Jr., General CPT -even dimension-five nonminimal couplings between fermions and photons yielding EDM and MDM, *Phys. Lett. B* **760**, 302 (2016).
- [40] J. B. Araujo, R. Casana, and M. M. Ferreira, Jr., Lorentz-violating contributions to the nuclear Schiff moment and nuclear EDM, *Phys. Rev. D* **97**, 055032 (2018).
- [41] J. B. Araujo, A. H. Blin, M. Sampaio, and M. M. Ferreira, Jr., Constraining dimension-six nonminimal Lorentz-violating electron-nucleon interactions with EDM physics, *Phys. Rev. D* **100**, 015046 (2019).
- [42] W. Hollik, J. I. Illana, S. Rigolin, C. Schappacher, and D. Stckinger, Top dipole form factors and loop-induced CP violation in supersymmetry, *Nucl. Phys. B* **551**, 3 (1999).
- [43] M. Nowakowski, E. A. Paschos, and J. M. Rodriguez, All electromagnetic form factors, *Eur. J. Phys.* **26**, 545 (2005).
- [44] C. Broggini, C. Giunti, and A. Studenikin, Electromagnetic properties of neutrinos, *Adv. High Energy Phys.* **2012**, 1 (2012).
- [45] F. Englert and R. Brout, Broken Symmetry and the Mass of Gauge Vector Mesons, *Phys. Rev. Lett.* **13**, 321 (1964).
- [46] P. W. Higgs, Broken symmetries, massless particles and gauge fields, *Phys. Lett.* **12**, 132 (1964).
- [47] P. W. Higgs, Broken Symmetries and the Masses of Gauge Bosons, *Phys. Rev. Lett.* **13**, 508 (1964).
- [48] M. E. Peskin and D. V. Schroeder, *An Introduction to Quantum Field Theory* (Perseus, Reading, 1995).
- [49] T.-P. Cheng and L.-F. Li, *Gauge Theory of Elementary Particle Physics* (Oxford University Press, Oxford, 1988).
- [50] C. Giunti and C. W. Kim, *Fundamentals of Neutrino Physics and Astrophysics* (Oxford University Press, New York, 2007).
- [51] P. Langacker, *The Standard Model and Beyond* (Taylor & Francis Group, Boca Raton, 2010).
- [52] M. D Schwartz, *Quantum Field Theory and the Standard Model* (Cambridge University Press, New York, 2014).
- [53] N. M. Monyonko, J. H. Reid, and A. Sen, Some properties of Green's functions in the non-linear R_ξ gauge, *Phys. Lett.* **136B**, 265 (1984).
- [54] N. M. Monyonko and J. H. Reid, One-loop vacuum polarization in the nonlinear R_ξ gauge, *Phys. Rev. D* **32**, 962 (1985).
- [55] J. C. Romo and A. Barroso, Renormalization of the electro-weak theory in the nonlinear gauge, *Phys. Rev. D* **35**, 2836 (1987).
- [56] J. G. Méndez and J. J. Toscano, A nonlinear R_ξ gauge for the electroweak theory, *Rev. Mex. Fis.* **50**, 346 (2004), <http://www.revistas.unam.mx/index.php/rmf/article/view/14008>.
- [57] A. I. Hernández-Juárez, J. Montañó, H. Novales-Sánchez, M. Salinas, J. J. Toscano, and O. Vázquez-Hernández, One-loop structure of the photon propagator in the standard model extension, *Phys. Rev. D* **99**, 013002 (2019).
- [58] V. A. Kostelecký and A. G. M. Pickering, Vacuum Photon Splitting in Lorentz-Violating Quantum Electrodynamics, *Phys. Rev. Lett.* **91**, 031801 (2003).
- [59] D. L. Anderson, M. Sher, and I. Turan, Lorentz and CPT violation in the Higgs sector, *Phys. Rev. D* **70**, 016001 (2004).
- [60] G. Bonneau, L. C. Costa, and J. L. Tomazelli, Vacuum polarisation effects in the Lorentz violating electrodynamics, *Int. J. Theor. Phys.* **47**, 1764 (2008).
- [61] M. A. López-Osorio, E. Martínez-Pascual, and J. J. Toscano, Implications of Lorentz violation on Higgs-mediated lepton flavor violation, *J. Phys. G* **43**, 025003 (2016).
- [62] G. Passarino and M. Veltman, One-loop corrections for e^+e^- annihilation into $\mu^+\mu^-$ in the Weinberg model, *Nucl. Phys.* **B160**, 151 (1979).
- [63] R. Mertig, M. Böhm, and A. Denner, FeynCalc—Computer-algebraic calculation of Feynman amplitudes, *Comput. Phys. Commun.* **64**, 345 (1991).
- [64] H. H. Patel, Package-X: A Mathematica package for the analytic calculation of one-loop integrals, *Comput. Phys. Commun.* **197**, 276 (2015).
- [65] R. P. Feynman, Space-time approach to quantum electrodynamics, *Phys. Rev.* **76**, 769 (1949).
- [66] C. G. Bollini and J. J. Giambiagi, Dimensional renormalization: The number of dimensions as a regularizing parameter, *Nuovo Cimento Soc. Ital. Fis.* **12B**, 20 (1972).
- [67] G. 't Hooft and M. Veltman, Scalar one-loop integrals, *Nucl. Phys.* **B153**, 365 (1979).
- [68] W. Gerlach and O. Stern, Der experimentelle Nachweis der Richtungsquantelung im Magnetfeld, *Z. Phys.* **9**, 349 (1922).
- [69] G. E. Uhlenbeck and S. Goudsmit, Ersetzung der Hypothese vom unmechanischen Zwang durch eine Forderung bezüglich des inneren Verhaltens jedes einzelnen Elektrons, *Naturwissenschaften* **13**, 953 (1925).
- [70] G. E. Uhlenbeck and S. Goudsmit, Spinning electrons and the structure of spectra, *Nature (London)* **117**, 264 (1926).
- [71] J. Schwinger, On quantum-electrodynamics and the magnetic moment of the electron, *Phys. Rev.* **73**, 416 (1948).
- [72] T. Aoyama, M. Hayakawa, T. Kinoshita, and M. Nio, Tenth-Order QED Contribution to the Electron $g-2$ and an Improved Value of the Fine Structure Constant, *Phys. Rev. Lett.* **109**, 111807 (2012).
- [73] T. Aoyama, M. Hayakawa, T. Kinoshita, and M. Nio, Complete Tenth-Order QED Contribution to the Muon $g-2$, *Phys. Rev. Lett.* **109**, 111808 (2012).
- [74] G. W. Bennett *et al.* (Muon $(g-2)$ Collaboration), Measurement of the Negative Muon Anomalous Magnetic Moment to 0.7 ppm, *Phys. Rev. Lett.* **92**, 161802 (2004).
- [75] D. Hanneke, S. Fogwell, and G. Gabrielse, New Measurement of the Electron Magnetic Moment and the Fine Structure Constant, *Phys. Rev. Lett.* **100**, 120801 (2008).
- [76] D. Hanneke, S. F. Hoogerheide, and G. Gabrielse, Cavity control of a single-electron quantum cyclotron: Measuring the electron magnetic moment, *Phys. Rev. A* **83**, 052122 (2011).

- [77] G. A. González-Sprinberg, A. Santamaria, and J. Vidal, Model independent bounds on the tau lepton electromagnetic and weak magnetic moments, *Nucl. Phys.* **B582**, 3 (2000).
- [78] A. D. Sakharov, Violation of CP invariance, C asymmetry, and baryon asymmetry of the Universe, *Pis'ma Zh. Eksp. Teor. Fiz.* **5**, 32 (1967) [*JETP Lett.* **5**, 24 (1967)]; Violation of CP invariance, C asymmetry, and baryon asymmetry of the Universe, *Usp. Fiz. Nauk* **161**, 61 (1991) [*Sov. Phys. Usp.* **34**, 392 (1991)].
- [79] B. Regan, E. Commins, C. Schmidt, and D. DeMille, New Limit on the Electron Electric Dipole Moment, *Phys. Rev. Lett.* **88**, 071805 (2002).
- [80] J. J. Hudson, D. M. Kara, B. E. Sauer, M. R. Tarbutt, and E. A. Hinds, Improved measurement of the shape of the electron, *Nature (London)* **473**, 493 (2011).
- [81] D. M. Kara, I. J. Smallman, J. J. Hudson, B. E. Sauer, M. R. Tarbutt, and E. A. Hinds, Measurement of the electron's electric dipole moment using YbF molecules: Methods and data analysis, *New J. Phys.* **14**, 103051 (2012).
- [82] J. Baron *et al.* (ACME Collaboration), Order of magnitude smaller limit on the electric dipole moment of the electron, *Science* **343**, 269 (2014).
- [83] M. Pospelov and A. Ritz, CKM benchmarks for electron electric dipole moment experiments, *Phys. Rev. D* **89**, 056006 (2014).
- [84] G. W. Bennett *et al.*, Improved limit on the muon electric dipole moment, *Phys. Rev. D* **80**, 052008 (2009).
- [85] K. Inami *et al.*, Search for the electric dipole moment of the τ lepton, *Phys. Lett. B* **551**, 16 (2003).
- [86] L. V. Avdeev and M. Yu. Kalmykov, Imaginary part of the electromagnetic lepton form factors, *Phys. Lett. B* **436**, 132 (1998).
- [87] P. Gambino and A. Sirlin, Relation between $\sin^2\hat{\theta}_W(m_Z)$ and $\sin^2\theta_{\text{eff}}^{\text{lept}}$, *Phys. Rev. D* **49**, R1160 (1994).
- [88] D. Binosi and V. Pascalutsa, The lifetime of unstable particles in electromagnetic fields, *J. Phys. G* **36**, 045001 (2009).